Naval Research Laboratory

Stennis Space Center, MS 39529-5004

NRL/MR/7330--07-8999

The Adriatic Circulation Experiment Winter 2002/2003 Mooring Data Report: A Case Study in ADCP Data Processing

JEFFREY W. BOOK
HENRY PERKINS

Ocean Sciences Branch
Oceanography Division

RICHARD P. SIGNELL

NATO Undersea Research Centre
La Spezia, Italy

MARK WIMBUSH

Graduate School of Oceanography
University of Rhode Island
Narragansett, Rhode Island

June 26, 2007

REPORT DOCUMENTATION PAGE

Form Approved
OMB No. 0704-0188

1. REPORT DATE *(DD-MM-YYYY)*	**2. REPORT TYPE**	**3. DATES COVERED** *(From - To)*
26-06-2007	Memorandum Report	

4. TITLE AND SUBTITLE

The Adriatic Circulation Experiment Winter 2002/2003 Mooring Data Report: A Case Study in ADCP Data Processing

5a. CONTRACT NUMBER

5b. GRANT NUMBER

5c. PROGRAM ELEMENT NUMBER
PE0602435N

6. AUTHOR(S)

Jeffrey W. Book, Henry Perkins, Richard P. Signell,* and Mark Wimbush†

5d. PROJECT NUMBER

5e. TASK NUMBER

5f. WORK UNIT NUMBER
73-6648-07-5

7. PERFORMING ORGANIZATION NAME(S) AND ADDRESS(ES)

Naval Research Laboratory
Oceanography Division
Stennis Space Center, MS 39529-5004

8. PERFORMING ORGANIZATION REPORT NUMBER

NRL/MR/7330--07-8999

9. SPONSORING / MONITORING AGENCY NAME(S) AND ADDRESS(ES)

Office of Naval Research
One Liberty Center
875 North Randolph St.
Arlington, VA 22203-1995

10. SPONSOR / MONITOR'S ACRONYM(S)

ONR

11. SPONSOR / MONITOR'S REPORT NUMBER(S)

12. DISTRIBUTION / AVAILABILITY STATEMENT

Approved for public release; distribution is unlimited.

13. SUPPLEMENTARY NOTES

*NATO Undersea Research Centre, Viale San Bartolomeo 400, 19138 La Spezia, Italy
†Graduate School of Oceanography, University of Rhode Island, Narragansett, Rhode Island

14. ABSTRACT

We present a case study of Acoustic Doppler Current Profiler (ADCP) data processing for long-term coastal deployments, using data collected by the Naval Research Laboratory and the NATO Undersea Research Centre from 14 trawl-resistant bottom moorings (BARNYs) during winter 2002/2003 across the northern Adriatic Sea. New methods were developed to maximize data quality and quantity. The data were truncated moving with the sea surface instead of using a constant level. An objective method based on horizontal velocity noise was developed for quality control of data using the ADCP error velocities. Tests were developed to reject fish-echo-contaminated data from an ADCP in which the fish-detection algorithm had been disabled. Spurious linear compass drifts were identified and corrected. In summary, this report documents the complete preparation of velocity, velocity error, temperature, pressure, echo intensity, surface wave, and salinity datasets from the ADCPs and wave/tide gauges in the main Adriatic Circulation Experiment.

15. SUBJECT TERMS

ADCP Adriatic Circulation Experiment
BARNY Data Processing

16. SECURITY CLASSIFICATION OF:			**17. LIMITATION OF ABSTRACT**	**18. NUMBER OF PAGES**	**19a. NAME OF RESPONSIBLE PERSON**
a. REPORT	**b. ABSTRACT**	**c. THIS PAGE**			Jeffrey Book
Unclassified	Unclassified	Unclassified	UL	50	**19b. TELEPHONE NUMBER** *(include area code)* (228) 688-5251

Standard Form 298 (Rev. 8-98)
Prescribed by ANSI Std. Z39.18

CONTENTS

1. INTRODUCTION 1

2. ADCP SETUP 2

3. ADCP PROCESSING 4
3.1 Measurement Start and End Times 4
3.2 ADCP Ringing and the Bottom Bin 5
3.3 Surface Side lobe Echo and the Top Bin 6
3.3.1 ADCP Vertical Range to the Sea Surface 6
3.3.2 Optimizing ADCP Vertical Range to the Sea Surface 7
3.3.3 Surface Truncation 8
3.4 Percent Good Quality Control 8
3.5 Internal ADCP Quality Control 9
3.6 Correlation Quality Control 10
3.7 Error Velocity Quality Control 10
3.7.1 Selection of Error Velocity Threshold 10
3.7.2 Application of Error Velocity Threshold 11
3.8 "Fishy" Ensemble Identification 12
3.8.1 Ensemble Fish Rejection 12
3.8.2 Fish Contamination at VR1 12
3.9 Compass Effects 13
3.9.1 Trawl Strikes and Storm-induced Slumping 13
3.9.2 Compass Drift 14
3.9.3 Heading Glitches 16
3.9.4 Magnetic Declination 16
3.9.5 VR5 Rotation 17
3.10 Missing Ensembles 18

4. ADCP FILTERED DATA 18
4.1 Depth 18
4.2 Velocity Data 19
4.3 Velocity Error Estimates 20
4.4 ADCP Temperature Data 21
4.5 Merging and Filtering VR1 data 22

5. ADCP AUXILIARY DATA 22
5.1 ADCP Pressure Data 23
5.2 ADCP Echo Intensity Data 23
5.3 VR1b ADCP Wave Data 23

6. WAVE/TIDE GAUGE DATA 24
6.1 WTG Pressure Data 24
6.2 WTG Temperature Data 25
6.3 WTG Salinity Data 25
6.4 WTG Wave Burst Data 26

7. DATA DVD 26

8. ACKNOWLEDGMENTS 27

9. REFERENCES 27

LIST OF FIGURES

1 Northern Adriatic Moorings for Winter 2002/2003 34
2 Comparison of Burst and Spread Sampling Schemes 35
3 Optimized ADCP Range and Backscatter Data 36
4 Velocity Scatter and std Ellipses vs. Error Velocity 37
5 Horizontal Velocity Noise vs. Error Velocity Threshold 38
6 Fishy Echo in Backscatter Data 39
7 Fish Contamination at VR1 40
8 Fish Contamination Removal at VR1 41
9 Heading and Compass Effects 42
10 Heading Time Series of JRP ADCPs 43
11 Half-Record Tidal Current Differences 44
12 Velocity Error Depth Correlations 45

LIST OF TABLES

1 Locations and Depths of Moorings. 29
2 Instrumentation and Measurement Periods 30
3 ADCP Settings. 30
4 Range to the Sea Surface from Pressure and Acoustics 31
5 Comparison of Measurements of Deployment Water Depth 32
6 Trawl Strikes and Compass Anomalies 33
7 ADCP Compass Corrections. 33

THE ADRIATIC CIRCULATION EXPERIMENT WINTER 2002/2003 MOORING DATA REPORT: A CASE STUDY IN ADCP DATA PROCESSING

1. INTRODUCTION

The Naval Research Laboratory (NRL) has funded the "Adriatic Circulation Experiment" (ACE) from October 2000 through September 2004 to study the effect of wind forcing on a shallow marginal sea. This project monitored the circulation and other physical aspects of a marginal sea over a winter period and compared these data with realistic high-resolution meteorological and ocean models. The northern Adriatic Sea was an ideal location for this study. The northern Adriatic is shallow (< 80 m) and is impacted in winter by strong cold winds called bora. These winds have been shown in various modeling studies to drive episodic circulation patterns. Bora also contribute to the formation in the northern Adriatic of the densest water to be found in the entire eastern Mediterranean Sea, North Adriatic Dense Water (NAdDW).

A specific objective of ACE was to measure the heat flux in the northern Adriatic over the winter of 2002-2003, and over various episodic wind events. Another objective of ACE was to map out and understand the winter circulation of the northern Adriatic at various time scales, i.e., mean, low frequency, inertial band energy, tidal fluctuations, etc.

To accomplish the observational objectives, bottom mounted Acoustic Doppler Current Profiler (ADCP) and hydrographic measurements were made in collaboration with the NATO Undersea Research Centre (NURC) as a Joint Research Project (JRP). JRP moorings consisted of 14 trawl resistant bottom mounted ADCPs (called BARNY moorings from their barnacle like shape) distributed along 4 moorings lines, three of which span the width of the Adriatic. Twelve of these ADCPs were provided by NRL and two were provided by NURC. An additional upward-looking ADCP (50% of the time from NRL and 50% of the time from NURC) was mounted near the base of a meteorological tower, Acqua Alta, and did not require a trawl resistant bottom mount. The locations of these moorings are given in Table 1 and shown in Figure 1.

These fifteen moorings were the most ever deployed at one time in the northern Adriatic, but were still not sufficient by themselves to provide complete coverage along the four mooring sections. To better address the observational objectives of the JRP, NRL and NURC entered into collaborative partnerships with several oceanographic laboratories (see Lee et al., 2005). These partnerships greatly expanded the variety and quantity of measurements that were made in the northern Adriatic over the winter of 2002-2003. Measurements made by JRP partners include hydrographic casts, surface drifter measurements, high-frequency radar measurements, meteorological platform and buoy measurements, towed body measurements, and current mooring measurements.

Manuscript approved March 30, 2007.

Current mooring deployments were jointly planned between NRL, NURC, and the collaborative partners such that the four mooring sections were completed by both JRP and partner moorings.

The 14 BARNY moorings were all deployed during a cruise of the R/V Alliance from September 16 through October 13, 2002. The ADCP near Acqua Alta was deployed on September 4, 2002, recovered and redeployed on December 18, 2002, and finally recovered on June 4, 2003. The other moorings were all recovered during another cruise of the R/V Alliance from April 23 through May 11, 2003. Two moorings (SS4, VR4) had early ADCP battery failure and one mooring (CP2) had a mechanical failure prior to recovery and therefore one month, one week, and one week of ADCP data were lost respectively to these problems. Table 2 gives complete details of mooring times of operation.

At the locations of the JRP moorings, measurements were made of currents throughout the water column (by ADCP), bottom temperature (by ADCP and at some sites by wave/tide gauge), and bottom pressure (by ADCP or wave/tide gauge). Additionally, at some locations, measurements were made of bottom salinity (by conductivity sensors), bottom pressure from surface waves (by wave/tide gauge), and surface wave parameters (by ADCP). Through the acoustic process of measuring water column currents, the ADCPs also provided data on backscatter echo intensity through the water column. Table 2 gives the details of mooring instrumentation.

2. ADCP SETUP

The setup for the JRP ADCPs was chosen to provide the most accurate hourly samples of water column currents possible for the extended ACE deployment (> seven months). Battery restrictions for the ADCPs allowed only 250-330 acoustic pings to be made during one hour. Research was conducted on how these pings should be distributed. Two different approaches were considered. The spread sampling approach distributes the allowed pings evenly throughout the hour, while the burst sampling approach uses all the allowed pings at a very fast sampling rate over a short period.

If a spread sampling approach had been used, the ping sampling period would have been 11-15 seconds. This aliases the wave portion (5-10 s) of the spectrum. For significant wave orbital velocities the estimate of the mean current for a particular hour would have high error especially near the surface. An example calculation showed a 5 cm/s error in estimation of the hourly mean for wave velocities of 100 cm/s superimposed on a 10 cm/s mean flow (Signell, Cavaleri, and Perkins, personal communication). Burst sampling at 1 Hz sampling frequency greatly reduces this error.

Nevertheless, burst sampling also introduces error in the estimation of hourly mean values. The aliased energy for burst sampling falls between the burst duration period and the period between bursts. To investigate this issue, the data from a JRP ADCP deployed by NURC near site SS6 during 2001 (Book et al., 2005) was examined. The mooring was deployed for less than two weeks and therefore was configured for a high sampling rate. The instrument used a spread sampling technique but saved ensembles every 5 minutes. Therefore these data could be used to estimate the spectral energy present at this site for periods between 10 minutes and 1 hour and how this energy would impact the hourly mean estimates for different sampling schemes.

Two hypothetical sampling schemes (Figure 2) were compared. Each value of the ADCP record (5 minute mean calculated by spread sampling) was used to represent what a burst sample would

measure. This time series was then sub-sampled at 65 minute intervals to simulate a sampling scheme (blue line in Figure 2) of burst pinging for 5 minutes every (approximate) hour. Some "spread sampling error" may still be introduced in these data because the sampling period is only 5 seconds, but such error should be reduced from the error that would be caused from an 11-15 s sampling rate. Also, this error was reduced by using measurements made at deeper depths (Figure 2 time series are from 33 m) where wave velocities have decayed to smaller values. Spread sampling (red line in Figure 2) was represented by averaging the 5 minute samples with the 6 samples before and the 6 samples after to form an average taken over 65 minutes. The hourly "burst" sample is not always a good representative of the hourly mean. This was especially true during the time when the currents were responding to a bora event (∼day 32).

To separate the error due to burst sampling from normal error reduction due to averaging, the difference between the time series in Figure 2 was assumed to be equal to a sampling error plus other random errors from the burst sampling time series plus the random errors of the spread sampling time series. Thus the variance of the time-series difference is equal to the sum of the variances of these error terms and then the standard deviation of the sampling error is

$$\sigma_{samp} = \sqrt{\sigma_{diff}^2 - \sigma_{inst}^2 - \frac{\sigma_{inst}^2}{13} + \frac{2\sigma_{inst}^2}{13}} \; . \tag{1}$$

In this equation σ_{diff}^2 is the variance of the difference time series (blue minus red in Figure 2), σ_{inst} is the expected instrument error in the "burst" sampling time series (blue line), and σ_{samp} is the error in the hourly mean due only to the choice of a burst sampling scheme. The last term in Equation 1 accounts for correlation between the errors of the burst sampling time series and the spread sampling time series since a portion of the data are shared. The value of the burst sampling error was estimated to be ±1.0 cm/s by using Equation 1 with the 2001 SS6 data and averaging all the σ_{samp} values for both u and v that were deeper than 23 meters (below the strong influence of surface wave contamination). Using another 2001 mooring deployed near site SS5, the calculated burst sampling error was again ±1.0 cm/s.

In estimating hourly means, the two sampling schemes have different types of errors. Spread sampling has the potential to generate high errors due to the presence of surface gravity waves. However this error decays with depth as the orbital velocities decay and will only be large during high wave conditions. Burst sampling has the potential to generate lower errors, but these errors will most likely be throughout the water column and present during much of the record. An ACE objective is to measure the transfer of energy to the ocean from high winds. Therefore burst sampling was used to minimize the error at the surface during storm conditions. However, to lower the burst sampling error, 4 bursts per hour were used instead of a single burst. The calculation to estimate the burst sampling error was repeated for this alternative sampling scheme with Equation 1 becoming

$$\sigma_{samp} = \sqrt{\sigma_{diff}^2 - \frac{\sigma_{inst}^2}{4} - \frac{\sigma_{inst}^2}{12} + \frac{\sigma_{inst}^2}{6}} \; , \tag{2}$$

for the "4-burst" average differenced with the hour spread sampling time series. For this case the calculated burst sampling errors were reduced to ±0.4 cm/s (10 m vertical error correlation length scale) and ±0.3 cm/s (5 m vertical error correlation length scale) for the SS6 and SS5 sites respectively.

Table 3 shows the burst durations for each JRP ADCP, which is equivalent to the number of acoustic pings at 1 Hz sampling frequency that made up each burst. All JRP ADCPs used the settings of ∼1 minute bursts of 1 Hz pings every 15 minutes except for VR1a which used 16 minute bursts of 0.5 Hz pings every hour. All JRP ADCPs used during this project were RD Instruments (RDI) Workhorse Sentinel broadband ADCPs with four acoustic beams set at a 20° angle to vertical. Most of the JRP ADCPs were 300 kHz instruments, but 600 kHz and 1200 kHz instruments were used at a few locations. These latter high frequency instruments allow more depth resolution and accurate measurements closer to the ADCP head at a sacrifice of measurement range. Table 3 shows the ADCP frequencies and bin sizes used at each site. In addition to the temperature and acoustic sensors common to all ADCPs, instruments at SS4, SS10, and VR1b contained pressure sensors. Temperature, pressure, and other measurements were made by the ADCPs with the same measurement timing and averaging as the velocity data. The instrument at VR1b used the RDI ADCP Waves Array Technique to measure surface wave parameters.

3. ADCP PROCESSING

ADCPs measure profiles of water column currents by measuring the Doppler shift from backscattered acoustic pings caused by the movement of suspended particles (biota, sediment) with the water velocity. A complete description of this technique is beyond the scope of this report. The Workhorse Technical Manual, Expert Command Guide, Broadband Primer, and ADCP Coordinate Transformation booklet provide such a description. This NRL report draws heavily on the information contained in these works. They are available from RDI as part of the Workhorse Documentation help file (version 1.0, 1999) and will be referenced in this report as RDI (1999).

Because of the complicated nature of the measurements, there are many possible sources of error that should be considered when processing ADCP data. The RDI Workhorse ADCPs output various status fields that can be used for quality control and data processing. This section discusses the sources of error present in the JRP ADCP data and the quality control and processing that was done to address these potential problems.

3.1 Measurement Start and End Times

The JRP ADCPs were all set to record their measurements internally and therefore they were turned on aboard ship before deployment and turned off aboard ship after recovery. Thus a simple initial step is to identify the start and end times of accurate water column measurements.

Most JRP ADCPs were lowered to the ocean bottom inside their trawl resistant BARNY moorings and then an acoustic signal was used to release the deployment tackle from the mooring. The first ensemble (burst) of measurement pings that began at least one minute after the tackle release command is used as the first good water velocity measurement and prior measurements are discarded.

For recovery, an acoustic command was sent to the BARNY mooring to release the buoyant donut float containing the ADCP from the mooring. If this standard recovery practice was successful then the ADCP floated to the surface and was recovered by the ship. For two instruments (SS4 and SS6), a backup release was used that released a larger buoyant portion of the mooring for surface recovery. Recovery by ROV was required at SS8 and VR2 where both recovery mechanisms failed.

CP2 had a mechanical mooring failure that released the ADCP buoyant donut prior to the ship's arrival. With the exception of this last mooring and the SS8 ROV recovery site, the last good water velocity measurement is taken as the last ensemble to complete at least one minute prior to the initial ADCP donut release command regardless of the recovery mechanism employed. All later measurements are discarded. At sites SS2 and VR6, where this particular time was not recorded, the requirement was for ensemble completion at least two minutes prior to the ADCP's arrival at the surface.

For CP2 (mooring failure), SS8 (ROV recovery on a different day), and VR1a/VR1b (diver deployment without a trawl resistant mount) the timing of the ADCP donut release command has no meaning or does not represent a change in ADCP measurement quality. For these three sites, the ADCP engineering data of pitch, roll, and heading and the recorded standard deviation[1] of these fields over an ensemble were used to determine when the mooring was fixed in the mount to start measurements (only at VR1a/VR1b) and/or released from a fixed position due to the particular mechanism of recovery.

All deployment and recovery truncations were checked against data quality to verify that the truncation points were accurately selected. The ADCPs at sites SS4 and VR4 ran out of battery energy (before recovery) and therefore no data are truncated from the end of these records by the procedure described above. The ADCPs record the time of the beginning of each ensemble of burst sampling. However for the purposes of further analysis (e.g., tidal analysis) it is preferable for the time to be given in terms of the center time of each ensemble of bursts. Therefore the ADCP time stamps were offset by half of a burst duration (Table 3) to move them to the centers of the ensembles.

The ADCP temperature measurements do not accurately reflect water temperatures immediately after mooring deployments. The ADCPs and moorings must cool or heat to approximate equilibrium with the bottom temperatures. Older ADCP models position their temperature sensors inside the ADCP housing while newer models measure temperatures just outside the ADCP housing. Therefore, equilibrium times differ from instrument to instrument. The temperature measurements from each instrument were examined to find the first point where temperature change stabilized or switched directions after deployment. Temperature readings prior to this point were marked as bad (see Section 4.4).

3.2 ADCP Ringing and the Bottom Bin

After transmitting an acoustic ping, the electronics of an ADCP ring from the transmission for a brief period (RDI, 1999). While it persists, this ringing contaminates the ADCPs ability to receive backscatter echoes. Because of this problem, the ADCPs were programmed to wait for a brief period for the ringing to decay before attempting to receive backscatter signals. The waiting period therefore becomes a blanking distance in which backscatter signal from scatterers close to the ADCP transducer head are ignored and no measurement of velocity is performed. The JRP ADCPs used the standard[2] RDI blanking distances of 176 cm, 88 cm, and 44 cm for the 300 kHz, 600 kHz, and 1200 kHz instruments respectively. No evidence of ringing contamination was found

[1] The standard deviation of the engineering fields was not recorded at VR1b
[2] VR1a used 40 cm instead of 44 cm

in the bottom bins above these blanking distances for the JRP ADCPs and therefore no bottom truncation of bins was done.

3.3 Surface Side lobe Echo and the Top Bin

The echo from the ocean surface from an ADCP acoustic ping is so much stronger than the echo from ocean scatterers that it can overwhelm the side lobe suppression of the transducer (RDI, 1999). The side lobe echo from the surface can propagate straight down and arrive at the transducer head at the same time as echoes from scatterers located just below the surface. This surface echo contaminates the measurements from these scatterers and therefore near-surface currents cannot be accurately measured. The height above the transducer head where contamination starts is simply the range from the ADCP transducer head to the surface multiplied by the cosine of the beam angle. Bins contaminated by surface echo should be truncated from the ADCP datasets as they contain false current signals.

Tidal fluctuations from ensemble to ensemble and wave fluctuation within an ensemble move the surface and hence the surface contamination zone. These processes spread the effect of the surface echo over depth and can also cause the elevation level of the contaminated bins to fluctuate significantly with time. If sea-surface height fluctuations are comparable to the ADCP bin size, than use of a fixed cutoff bin for all measurement times will either accept contaminated data at low sea-surface height times or truncate good data at high sea-surface height times, or do both. Due to the interest in near-surface processes from JRP data, truncation of surface bins for JRP ADCPs was instead allowed to change with time, following the sea-surface height.

3.3.1 ADCP Vertical Range to the Sea Surface

In order to calculate which bins the surface echo contaminates for a given time, we need an accurate estimate of the fluctuating sea-surface height above the ADCP transducer head. Most ADCP moorings also contained wave/tide gauges (see Section 6) which measured the bottom pressure at time intervals comparable to ADCP measurement intervals. Three of the ADCPs were not deployed with wave/tide gauges but instead the ADCPs themselves measured bottom pressure. No bottom pressure measurements were made at site VR1a.

Atmospheric pressure contributes to the measured bottom pressures and must be removed from the bottom pressure measurements before using them to calculate sea-surface height. Atmospheric pressure was measured at several AGIP gas platforms spread around the northern Adriatic Sea and a mean time series was estimated by averaging the atmospheric pressure from six of these platforms[3]. Various offsets were found from different wave/tide gauges by comparing this mean atmospheric pressure time series to the measurements of atmospheric pressure made by the mooring gauges while they were still on the ship deck. The offsets ranging from -1 to 9 cm are assumed to be caused by pressure gauge bias and therefore both these offsets and the oil platform atmospheric pressure time series are subtracted from the bottom pressure time series to obtain bottom pressure time series due only to water head.

To convert the corrected bottom "water-pressure" fields to height fields, a time series of average water column density was estimated using the measured temperatures (at the bottom), a constant

[3]Ada, Annabella, BarbaraC, GaribaldiA, Giovanna, and Pennina

salinity value of 38.2 psu (the average of three bottom salinity time series, see Section 6.3), and half the bottom water pressure. The range from the pressure gauge to the surface was assumed to be given by the hydrostatic relation and thus equal to the corrected bottom "water-pressure" field divided by the gravitational acceleration and this density. Based on the physical dimensions of the BARNY moorings, the wave/tide pressure sensors were assumed to lie 0.4 m below the ADCP transducer heads.

Moorings SS4, SS10, and VR1 did not have wave/tide gauges. However, the ADCPs at SS4, SS10, and VR1b contained pressure sensors. The ADCP automatically sets "zero" pressure as the measured pressure when it is turned on. To remove the effects of atmospheric pressure from the ADCP measured pressure, the time series of average atmospheric pressure from the six gas platform measurements was subtracted from the ADCP pressure time series. Then an offset was added to force the mean of the "water-pressure" time series to be zero before deployment. The range from the ADCP to the surface for these instruments was calculated with the hydrostatic assumption in the same manner as was done for the wave/tide gauges. However the level of these pressure measurements is directly at the level of the ADCP transducer head instead of 0.4 m below.

3.3.2 Optimizing ADCP Vertical Range to the Sea Surface

A rough measure of the vertical range from the ADCP transducer head to the surface is provided by the ADCP backscatter data as the surface echo is usually many times stronger than other echoes and therefore the bin containing the surface can be identified as the bin with the maximum backscatter intensity. The disadvantages of using these time series for surface truncation are the poor depth resolutions (bin size) and the occasional times when the surface echoes become unclear or disappear.

A comparison of the pressure-derived range time series and the acoustic-derived time series (Table 4) shows that the means of the pressure-derived time series are greater by more than 35 cm for all sites with 300 kHz ADCPs. The two sites with 600 kHz and 1200 kHz ADCPs and smaller bin sizes (SS2 and VR1b) have smaller differences, but the pressure-derived means are still greater than the acoustic-derived means by 18 and 14 cm respectively. Possible explanations for the fact that the pressure time-series means are greater for all sites include instrument error (stress-induced, pressure-gauge bias), sound-speed variations within the water column (ADCPs estimate sound speed from bottom temperature), or preferential acoustic reflection from wave troughs.

Further comparisons of different methods of estimating range to the surface can be made for the specific time of the ADCP deployment. During this time, the ship's echo sounder provides an estimate of the distance between the sea-surface and the bottom. Also, CTD data can be used to correct the acoustic-derived estimate with the real sound-speed profile and to correct the pressure-derived depth time series with the actual average water column density. Table 5 shows a comparison of these three independent estimates of total water column depth[4].

The mismatch between the two range time series prevents the direct use of the pressure-derived range time series for determining a truncation distance below the acoustic surface echo. However, removing a constant offset from the pressure-derived time series can bring the two time series

[4]the pressure- and acoustic-derived estimates of ADCP range were adjusted by 0.5 m to account for the height of the BARNY mooring

into alignment and then the pressure-derived ranges can be used. To calculate the offset, a "first-guess" was made such that each pressure-derived time series was adjusted so that its mean agreed with the mean of the acoustic-derived time series. Then, because of problems with surface echo determination in the acoustic-derived time series, values above the maximum and values below the minimum of the first-guess time series were discarded in the acoustic-derived time series. Both time series were discretized to bin numbers and a cost function was calculated as the sum of the squared difference between the resulting time series. The first-guess time series was adjusted in increments of 1 cm through the range of one half of a bin size below its original minimum to one half a bin size above its original maximum. After each adjustment, the discretization was performed and a new cost function was calculated. The adjusted time series with the lowest cost function was taken as the optimized time series (see Table 5). Finally, if the new "optimized" time series would have had different acoustic-derived time-series discards than the "first-guess," or the mean of the "optimized" time series was within 1/6th of a bin center when all but two bins were discarded, then the optimization was repeated with different acoustic-derived time-series discards derived from the "optimized" time series in the first case or expanded to three bins centered on the mean of the "optimized" time series in the latter case. Figure 3 shows an example of the optimally adjusted pressure-derived range time series superimposed on the backscatter intensity field.

Bottom pressure was not measured at mooring VR1a. However, the bin size for this instrument was only 35 cm and therefore the acoustic-derived range time series was not as poorly resolved in depth as at the other sites. For a better representation of this time series during times of unclear surface echoes, values from the time series were discarded if the backscatter intensity fell below 90 dB and the estimated range was less than 15.8 m. The discarded values were filled in through linear interpolation and the result was used as the *optimized* time series. 3% of the points in the (hourly) time series were replaced in this way.

Moorings SS10, KB1, and VR4 did not have enough bins to measure beyond the sea-surface and therefore acoustic-derived range time series could not be calculated for these sites. Therefore at these sites, the pressure-derived range time series were offset by deployment sound-speed corrections and -0.25 m, the mean difference between the optimized and pressure-derived, deployment sound-speed corrected time series for the other 300 and 600 kHz ADCP sites[5] (see Table 5).

3.3.3 Surface Truncation

Geometrically, the straight surface echo will arrive at the ADCP transducer head at the same time as echoes at a distance equal to the total range to the surface multiplied by the cosine of the beam angle. For each time, this distance was calculated using the optimized total range time series, and the bin where this contamination occurred and all bins nearer to the surface were discarded. Thus, a constant distance from the moving sea-surface was used for truncation at all times. The beam angle for all JRP ADCPs is 20° and therefore the truncated, unusable portion is 6% of the water column.

3.4 Percent Good Quality Control

The Janus configured RDI ADCPs use four acoustic beams and measure the water velocity component parallel to each beam. A correlation test is performed on each of the echoes and the

[5]Site VR2 was not used in this average because the deployment sound-speed correction was not available.

velocity components parallel to beams with echoes that fail this test (correlation count below 64) are marked as bad (RDI, 1999). Another test is performed on the echoes to detect the presence of strong targets (fish) in some beams that will compromise the velocity estimates (RDI, 1999). Velocities from beams with echoes that fail this test are also marked as bad. If all four velocity components pass the tests, the ADCP can combine them to produce east/west velocity, north/south velocity, and two independent measures of vertical velocity (RDI, 1999). If three velocity components pass, the ADCP can still combine them to produce east/west, north/south, and vertical velocity.

This process is repeated for each acoustic ping over all the depth bins and the calculated velocities are averaged over an ensemble of pings to produce the final stored velocities. For each depth bin and each ensemble the ADCP also stores the percentage of pings in the ensemble for which a three-beam solution was applied (% good field 1), for which the velocity solution fails an error threshold test (% good field 2, see Section 3.5), for which more than one beam failed the correlation or fish test (% good field 3), and for which a four-beam solution was applied (% good field 4).

A high percentage of pings without velocity solutions indicates that conditions were not favorable for ADCP velocity measurements at that particular time and depth level. For these cases, because the tests are not perfect, the pings that do pass the tests might also be contaminated by the same environmental factors that are causing other pings to fail the tests. Therefore by inspection of the JRP ADCP data it was determined that ensembles with less than 60% solutions[6] should be marked as bad for this dataset. The velocities from these ensembles were not used in further processing steps.

There is a higher probability of environmental contamination of pings from the near-surface zone than from elsewhere in the water column. In particular, the top bin is more likely to be affected by surface generated bubbles and could be contaminated in part or in whole by the surface side lobe echo (surface movements within an ensemble burst or an error in selection of the surface truncation level for a particular ensemble). For these reasons, an 80% solution threshold was used for the top bin of each time sample rather than the 60% threshold used for other bins.

3.5 Internal ADCP Quality Control

The two independent measures of vertical velocity from four-beam solutions are subtracted and weighted to produce an "error" velocity for each ping. The weighting is such that the variance of the error velocity should match the variance of the horizontal velocity attributable to instrument or environmental noise (RDI, 1999). If the error velocity from a ping exceeds a certain threshold then the velocity solution from that ping is marked as bad (% good field 2). For the JRP ADCP data, the RDI default was used and almost no pings failed this threshold (200 cm/s) test. After recovery, further quality control was done using an ensemble velocity error threshold particular to each instrument (see Section 3.7).

An RDI ADCP does not produce solutions for pings that fail the error velocity test or for pings that have two or more beams fail the RDI correlation and fish tests (see Section 3.4). If all the pings in the ensemble do not produce velocity solutions (% good field 2 plus % good field 3 equals 100%), the ensemble is marked as bad. For the JRP ADCPs this situation almost never occurs

[6] % good field 1 plus % good field 4

because of the high error velocity threshold and the quantity of pings per ensemble. No velocities are available or used from the few ensembles where this does occur.

3.6 Correlation Quality Control

High signal-to-noise ratios for ADCP measurements should produce correlation counts around 128 (RDI, 1999). Low signal-to-noise ratios will produce low correlation counts. Indirect quality control is applied to low correlations through the internal ADCP rejection of pings with low correlation counts on more than a single beam and through the applied percent good quality control which rejects ensembles with high percentages of such rejected pings.

However, a small number of ensembles will pass these RDI tests with low ensemble averaged correlations. The velocities for these ensembles can be unrealistic. Therefore, for the JRP ADCP data, if the correlation count average over the four beams was less than 64 counts for a depth bin, that ensemble was marked as bad and not used in this dataset. Less than 1% of ensembles at any site failed this quality control test and some of these ensembles also failed other tests.

3.7 Error Velocity Quality Control

As discussed in Section 3.5, for the JRP ADCP data the error velocity threshold was set to such a high value that almost no data were rejected by the internal error velocity test. This is the default setting and gives the user the most control over this type of quality control procedure.

Error velocity magnitudes can become high through statistical chance, through violation of the homogeneity assumption across ADCP beams (RDI, 1999), or through velocity contamination from non-standard environmental factors (bubbles, fish, etc.). Ensembles with high error velocity through statistical chance should not be rejected (i.e., there is a finite statistical probability that the two independent measures of vertical velocity will disagree when horizontal velocities are as accurate as at other times). However, non-standard environmental factors that cause very high error velocities are also likely to cause very high error in horizontal velocity estimates and these ensembles should be rejected. As the error velocity magnitude increases, statistical chance becomes less likely as the culprit for the errors.

3.7.1 Selection of Error Velocity Threshold

A threshold error velocity magnitude value is needed that will eliminate excessively noisy and bad data but not exclude too many ensembles that have high error velocities through normal statistical chance. A threshold can be objectively determined using the assumption that the ocean signal variance is uncorrelated to error velocities. This is not likely to be strictly true but still provides a better alternative to selecting an arbitrary threshold.

The basic method is to separate the entire horizontal velocity dataset for a particular instrument into a series of subsets based on error velocity magnitude[7] (e.g., ensembles with error velocity magnitudes less than 5 cm/s, ensembles with error velocities greater than or equal to 5 cm/s but

[7]Ensembles with 90% of pings forming three-beam solutions were automatically categorized in the subset of lowest error velocity magnitude regardless of their actual error velocity value since such values would be highly inaccurate due to the lack of four-beam solutions.

less than 6 cm/s, etc.). Then the variance of the horizontal velocities of each subset is assumed to be equal to the sum of an ocean signal variance (assumed constant across subsets) plus the noise variance for that particular subset. Thus the increase in noise variance with increasing error velocity thresholds can be estimated and a cutoff can be chosen based on a desired maximum noise variance.

The first step in applying the method to the JRP ADCP data is to estimate the ocean signal variance for each instrument. For all subsets this variance is combined with some level of noise variance. RDI planning software provides a theoretical noise standard deviation for horizontal velocity measurements (Table 3) based only on the number of pings per ensemble, the ADCP bin size, and the ADCP frequency. Discussion of this estimate is beyond the scope of this report (see RDI, 1999) but it should be approximately accurate in the absence of non-standard environmental factors. Therefore the subset of ensembles with the lowest velocity error magnitudes is assumed to have this theoretical noise variance because they are least likely to be affected by such factors. I.e., the ocean signal variance for an instrument was calculated as the total variance of the lowest error subset minus the theoretical noise variance. Based on the general distribution of error velocity magnitudes, 5 cm/s was used as the cutoff for the lowest velocity error magnitude subset for all instruments except ADCPs at SS2, VR1a, and VR1b, where 4, 1, and 3 cm/s were used respectively[8].

Once the ocean signal variance was estimated from the first subset, the noise variances for each subsequent (1 cm/s bins) error subset was calculated as the total variance for the subset minus this ocean signal variance. This was repeated for both the major and minor axes of variation. Figure 4 shows a graphical example of this analysis. For each mooring, the result was a functional relation[9] between horizontal-velocity noise standard deviation (major and minor axes) and error velocity magnitude (Figure 5).

An objective standard can be chosen based on horizontal-velocity noise standard deviation since it is clear that data should be rejected if the error exceeds the error that would be generated if such data were filled in by interpolation from surrounding data. The average value from the estimates of data gap interpolation error is close to 5 cm/s (Section 4.3). Therefore using the functions from Figure 5, the error velocity threshold for each instrument was chosen such that the associated horizontal velocity noise standard deviation did not exceed 5 cm/s for either the major or minor axes[10] of variation.

3.7.2 Application of Error Velocity Threshold

Table 3 shows the calculated error velocity thresholds for the JRP ADCPs. Ensembles with error velocity magnitudes greater than or equal to these values were marked as bad. This quality control test was not applied to ensembles with 90% or more of the ensemble pings producing 3-beam solutions. For such very uncommon ensembles, the error velocity field is expected to be unreliable

[8]The general quality of the data at these sites is higher and thus more of the error velocity magnitude distribution is concentrated below 5 cm/s

[9]smoothed to avoid relative maximums.

[10]VR1a had a small group of strong flows directed off the minor axis with error velocities magnitudes higher than 1 cm/s (the lowest subset). Perhaps these flows are from residual fish contamination (see Section 3.8.2), but regardless they skew and invalidate the minor axis test. For VR1a only, the error velocity cutoff threshold was determined only using the major axis direction of variation.

as an indicator of velocity data quality because other velocity fields were predominately determined from pings not used to produce the error velocity field. Although the error velocity thresholds vary significantly from instrument to instrument, the level of noise variance that was excluded should be approximately equal for all instruments under the assumptions of Section 3.7.1.

3.8 "Fishy" Ensemble Identification

As discussed in Sections 3.4 and 3.5, the internal processing of the ADCPs identifies and rejects beams that show evidence of contamination by strong targets such as pelagic fish. The ADCP uses differences between the backscatter intensities along the four separate beams to identify one or more beams with anomalous scatterers (RDI, 1999). However, if the target strength of the "fish" is strong enough, the echo will interact with the side lobes of the other beams and could affect the backscatter intensity of all the beams. For these cases, the error velocity will be low (RDI, 1999), the fish detection algorithm may fail to reject the ping, and the velocities will be contaminated by the motion of the fish. Such ensembles can however be identified by the spike in time of the backscatter intensity produced by the fish.

3.8.1 Ensemble Fish Rejection

For all instruments except VR1a and VR1b, ensembles with a 20 dB or more increase in backscatter intensity immediately followed by a 20 dB or more decrease in backscatter intensity along a depth bin were marked as bad. The threshold of 20 dB was selected by inspection of records with spikes in backscatter intensity and spikes in velocity. Figure 6 shows a typical example of a "fishy" backscatter signal.

3.8.2 Fish Contamination at VR1

Unfortunately, the internal ADCP fish detection algorithm was disabled for VR1a and VR1b ADCPs. These records contain numerous clear examples of contamination (Figure 7). RDI (1999) and Plimpton et al. (2000) state that fish contamination biases velocities towards zero. However, at VR1a and VR1b velocities did not appear to be biased toward zero but instead unusual correlations were created between the four velocity fields. The reason for these correlations is unknown. They could possibly be related to the preferred positioning of fish schools around nearby structure and the exact path of particular ADCP beams. Regardless of the cause, these ensembles should be identified and rejected, but the test from Section 3.8.1 is insufficient for this task because of the level of contamination (6% of data). The structure of one of the unusual correlations was used to identify these contaminated ensembles.

The upper-left panel of Figure 8 shows the relationship between vertical velocity and error velocity for VR1a. Superimposed on a normal elliptical scatter is a trend of high positive vertical velocities and high error velocity magnitudes. To remove these bad ensembles, first all positive vertical velocity ensembles were temporarily discarded from the vertical velocity and error velocity datasets. Then the remaining data were duplicated and reflected across the line of zero vertical velocity to produce a new symmetric vertical/error velocity dataset. Standard-deviation ellipse parameters were calculated from this dataset. Returning to the original vertical/error velocity data, ensembles were marked if they fell outside the four-standard-deviation ellipse calculated from the reflected dataset. Data inside this ellipse are marked with a black point in the upper-right panel of Figure 8.

Points outside the ellipse are marked as bad if they have positive vertical velocities and their error velocity magnitudes exceed 1 cm/s. Excluded data are marked as red points in the bottom-left panel of Figure 8. This procedure eliminates most of the fish contaminated data from VR1a and VR1b.

3.9 Compass Effects

RDI ADCPs measure velocities in a coordinate system with respect to the ADCP itself. However, with internal processing these velocities are converted to an Earth referenced system for scientific use. One step in the conversion is a rotation of the velocities based on the measured ADCP heading such that the "v" component of velocity aligns with magnetic north. For self recording ADCPs such as those used during the JRP, the heading for this rotation is provided by an internal flux-gate compass (RDI, 1999). Before deployment, but after battery replacement, a compass calibration was done for each ADCP compass to correct for the distortions caused by the battery itself. Calibration is repeated until the overall error from a measurement at every 5° for a full 360° rotation is less than 5° (RDI, 1999).

Once deployed in a fixed bottom mount, the heading from the flux-gate compass should remain constant until recovery. Departures from this can be explained by one of four effects: (1) actual mooring movement, (2) changes in the magnetic field of the ADCP, (3) electronic noise and drift in the compass, and (4) changes in the Earth's magnetic field. Effects 2–4 can lead to velocity errors since they will cause errors in the ADCP's measurement of the direction of magnetic north with respect to the ADCP beams and therefore incorrect rotations in the conversion to Earth coordinates. Effect 1 does not cause such problems since it comes from a correct measurement of a rotation of the ADCP itself. However, these rotations should be identified in order to distinguish them from the other three effects, and in particular to measure and correct for electronic compass drift.

3.9.1 Trawl Strikes and Storm-induced Slumping

Mooring movement can be divided into three categories: (1) settling following deployment, (2) movement from strikes by fishing trawls and equipment, and (3) slumping from sediment scouring due to strong currents induced by storms. Movement in category 2 is the most obvious. When struck by a fishing trawl, the BARNY mount tends to undergo an impulse rotation, i.e., a large change in heading between two ensembles with zero heading standard deviation for each of these ensembles. On rare occasions, the trawl strike will take place in the middle of an ADCP ensemble and thus there will be a large change in heading over three ensembles with the middle ensemble having non-zero heading standard deviation and the other ensembles with zero heading standard deviation. Table 6 summarizes the trawl strikes found in the JRP ADCP data. Most of these were found by taking a taking a 5 point median filter of the ADCP heading and searching for impulse changes in the filtered data of more than 0.2°. This test was applied from 100 hours after the ADCP was turned on until 25 hours before the ADCP was turned off to avoid ship-deck time, deployment and recovery times, and movement in category 1. The test is likely to be a conservative estimator of trawl strikes as some strikes could move the BARNY less substantially and have smaller heading rotations or only pitch and roll changes. There was one small heading rotation each for SS2 and CP2 that was compelling enough by inspection to count as a trawl strike in Table 6. A few pitch and roll impulse shifts in SS5 and CP2 without accompanying heading shifts may have been trawl

strikes but were not counted as such because of limited evidence distinguishing these from storm slumping movement.

Throughout the ADCP records there are many examples of mooring movement induced by storms (category 3). These movements have similar magnitudes to those of trawl-strike movements (category 2) but can usually be clearly distinguished because storm movement tends to take place over a period of hours instead of abrupt changes from ensemble to ensemble. For example, some slumping events show the amount of rotation increasing with time every ensemble until a sudden large rotation occurs. Also, storm induced rotation can affect several moorings at nearly the same time, as the dynamics of sediment scouring and mooring slumping will be common to multiple sites. In particular the strong sirocco storm (along-axis southeast winds) of Nov. 16–17 produced such a response with significant rotations at sites SS9, VR1, VR2, and VR6 and movement at SS6 and SS10. In contrast, response to the strong bora storm of Jan. 7 was only seen at VR1 and only with a shift in pitch and roll. This suggests that the response might be correlated with wave activity as the sirocco storms in general have more significant waves than bora storms because they have longer fetch. Response at site VR1 was much more dramatic than at other sites as its deployment frame was not as resistive to slumping as the BARNY mounts used elsewhere. Other events with characteristics suggesting storm causes occurred on Sep. 9 (VR1), Oct. 2–3 (VR4), Oct. 22 (VR1), Nov. 13 (SS2), Nov. 22 (VR2), and Apr. 22-23 (SS9). A listing of the events by mooring is provided in Table 6.

3.9.2 Compass Drift

Any change in the recorded ADCP heading that is not a real mooring movement (i.e., effects 2–4) results in velocity directional errors in the conversion from beam coordinates to Earth coordinates. For many sites there are periods of nearly linear change in the heading that cannot be easily explained by mooring movement. Although this drift is presumably spurious, we do not know its cause. As seen in Figure 9, CP3 is a particularly clear example of this effect. The blue trace (over-plotted by red in places) shows the raw heading. The 7° shift on day 429 (Mar. 6, 2003) is the single trawl strike seen at this site. The red trace shows the heading with this jump removed to highlight graphically the low-frequency drift. The black trace shows the resulting heading if linear trends are removed piecewise before and after the trawl strike. This illustrates how the horizontal velocities are corrected for the compass drift. u and v are gradually rotated with time to compensate for the shifting of the ADCP heading away from magnetic north. Thus the assumption is that the ADCP heading correctly identified magnetic north when deployed and that the linear rotation observed afterwards is false.

Table 7 shows the total u and v velocity rotations applied at each mooring to correct for the compass drift. At sites SS5, SS9, KB1, VR1a, VR4, and VR6, where drift was not apparent or less than 1°, no correction was applied. CP3 is a particularly simple case, but other sites had linear drift that was more complicated. Drift seemed to suddenly start or stop at particular times and sometimes inflect after trawl strikes. Therefore drift correction was done piecewise between trawl strikes and certain drift inflection points identified by eye (given in Table 6). Drift did not have a standard pattern with linear drift occurring before the inflection point for SS4, in-between inflection points for SS8 and VR5, and after the inflection point for SS2, SS10, and VR2. For these ADCPs the drift correction was only applied in the portion of the record with clear linear drift. At sites SS6, CP2, CP3, and VR1b, drift was nearly linear and constant throughout the record.

Figure 10 shows all the ADCP heading records with their trawl-strikes, drifts, storm slumps, and other effects.

Two different tests were conducted to verify that the linear drifts in the compass headings were in fact false trends and therefore should be removed. The first was to assimilate tidally analyzed vertically-averaged currents and bottom pressures into a shallow-water, variational strong-constraint data assimilation model (see Section 3.9.5) with and without the compass drift correction. VR5 current data were excluded from this test for reasons explained in Section 3.9.5. In this test, the uncorrected dataset performed slightly better with a total rms (over time and station) decrease of 0.003 cm in surface height and 0.008 cm/s in tidal currents. The model simulated tides were nearly identical for both cases and most of the small error increase resulted from currents at sites SS6, CP2, and CP3, which were rotated away from the stable model solution by the correction. Considering uncertainty of the model, these improvements were not compelling enough to warrant elimination of the compass drift correction, especially given the results of the second test.

The second test was to calculate tidal ellipse parameters from both the first and second half of the vertically-averaged current time series, with and without compass drift corrections. Each half of the time series was tidally analyzed using the response method (see Section 4.2) and then the tidal ellipse tilt values were compared. This test should be sensitive to compass rotations as either an uncorrected compass drift or an improperly detrended compass record will cause different ellipse orientations in each half for the same barotropic tide. Also different versions of tidal currents for the first half of the time series were reconstructed from tidal coefficient estimates calculated from either the first or second half analysis. Vector differences were then calculated from these and the average magnitude of the vector difference was compared for cases with and without compass drift corrections.

The results are shown in Figure 11. The top panel shows the average vector difference magnitude from the case without compass drift corrections minus the average vector difference magnitude from the case with compass drift corrections. A positive value indicates that compass drift corrections decreased the differences in tidal currents reconstructed from the first and second half analyses. Sites SS6, SS8, CP2, and CP3 had large decreases in this error term, sites VR1b and VR2 had small decreases, and sites SS2, SS4, SS10, and VR5 had small increases in this error. In the bottom panel, the red trace is the absolute difference in M_2 ellipse orientation between the first and second halves from the uncorrected time series, and the blue trace is from the corrected time series. The sites with the four largest drift corrections (SS6, SS8, CP2, and CP3) all show marked improvement with relatively high values of ellipse orientation difference dropping significantly to levels similar to other sites. Sites SS2 and SS4 also showed improvement, but sites SS10, VR1b, VR2, and VR5 had larger differences after correction. The differences in ellipse orientation determined from the first and second halves of VR1a and VR1b are larger than those for the other sites, because these two half time series are approximately half the length of the others and therefore ellipse orientation uncertainty is higher.

The half-record tide test provides compelling evidence in support of a compass drift correction for sites SS6, SS8, CP2, and CP3, while results for other sites is mixed. However, compass drift correction is made at the other sites as detailed in Table 7 since the test supported the concept of the correction and it might not have been sensitive enough to detect improvements from smaller rotations.

What causes these drifts? Changes in the Earth's magnetic field (effect 4) are too small to account for such large drifts. In this region the long-term change should only be $\sim 0.07°$ counter-clockwise rotation per year and the short-term changes can clearly be seen as high-frequency semi-periodic noise (e.g., see black trace of Figure 9) in the ADCP headings, correlated between sites[11]. These data provide no information to distinguish between magnetic (effect 2) and electronic noise (effect 3) causes of linear drift. However, some suspicion rests on magnetic field changes from the draining ADCP battery pack over a deployment. This has not been demonstrated before according to RDI (personal communication) and we cannot determine this as the definitive cause. But recent deployments may offer further evidence in support of this theory as linear heading drift was observed with about the same overall magnitude but in a much shorter period from an ADCP that sampled enough to drain a battery pack in a month.

3.9.3 Heading Glitches

For the ADCP heading records there are a small number of single point positive or negative spikes in heading from the normal values. Some of these are associated with non-zero heading standard deviations (i.e., the compass heading was changing within the duration of an ensemble) but zero pitch and roll standard deviations, and therefore are not likely caused by real mooring movement. Examples of such spikes are the two positive spikes in Figure 9 on days 324 and 403. There is a risk that the current direction for such an ensemble could be compromised since an unknown electronic or magnetic glitch must have affected the compass data for at least one ping. Therefore, the velocity data are marked as bad for these rare ensembles. The number of glitches found and marked bad were 1 for SS2, 2 for CP3 and VR4, 4 for VR2, 5 for VR5, 6 for VR6, and none for all other instruments. No quality control is applied for ensembles with spikes in compass heading with zero heading standard deviations.

3.9.4 Magnetic Declination

RDI ADCPs use an internal flux-gate compass to measure the angle between beam three and magnetic north and then use this result to convert ADCP measured velocities to an Earth referenced system with positive v velocities pointing towards magnetic north. To convert them to a true (geographical) north reference, the coordinate system must be rotated by an amount given by the local magnetic declination at the site.

To find magnetic declination, the program pmaggrid30.exe was obtained from the National Geophysical Data Center of the National Oceanic and Atmospheric Administration and run using the 2000 International Geomagnetic Reference Field. Two dates were run for a grid of 12–20°E longitude, 38–46°N latitude, and zero elevation. The dates were September 20, 2002 and May 6, 2003, and then these two grids are averaged together to produce a magnetic declination grid for the JRP period. For each ADCP, a single declination value was found by linear interpolation from this grid and then all the horizontal velocities were rotated by this amount to convert to a true north reference system. Table 7 shows the rotation angles that were used. For all cases, magnetic north is east of true north and thus a clockwise rotation of the velocity vectors is required to reference to the new coordinate system that is counter-clockwise rotated from the old coordinate system.

[11] e.g., 2-day high-pass-filter heading time series at CP2 and VR6 are correlated with a correlation coefficient of 0.87

3.9.5 VR5 Rotation

During research work on northern Adriatic tides using JRP data, Janeković and Kuzmić (personal communication) noticed that tidal ellipses computed from ADCP measurements at site VR5 were strongly tilted with respect to tidal ellipses at neighboring stations. Also they observed that VR5 ellipses did not agree with predictions from their tidal simulation using the finite element model "Truxton/Fundy" (Janeković and Kuzmić, 2005). A separate comparison was done between measured and modeled tidal ellipses using the tidal component of simulations from the Navy Coastal Ocean Model (NCOM) (Martin et al., 2006). Again, all stations matched well except for VR5 which had an approximate 30° counter-clockwise tilt in the measurement ellipse relative to the simulated one.

The Truxton/Fundy simulation was forced with boundary conditions determined through data assimilation of analyzed data from six long-term coastal tide stations and the NCOM simulation was forced by data from the Oregon State University tidal databases which were originally derived through data assimilation of satellite altimetry. Neither of these methods assimilate current data, so to explore if the 23° to 27° tidal current directional difference between VR5 and VR4/VR6 could be dynamically reasonable a third data assimilation model was used. Following the technique described by Griffin and Thompson (1996), a strong-constraint variational data assimilation scheme was applied to the vertically averaged tides derived from all the JRP moorings. The model was set up with a 45° CCW rotated Arakawa C grid using 2 km bathymetric resolution (4 km resolution for u, v, and η). The bathymetric grid was derived from the NURC 7.5-second Adriatic database (Bardini, personal communication) by averaging over $\sqrt{2}$ km square blocks and then using nearest-neighbor interpolation to the 2 km tilted square grid. The centers of the tilted grid align with every other diagonal of the finer resolution untilted grid, and thus the nearest-neighbor interpolation is effectively done by selecting every other grid point, staggered every row or column (i.e., selecting along diagonals of the finer grid). The model is forced by 18 time-dependent structure functions along the southeastern boundary ([43.5386°N, 13.2569°E] to [44.7839°N, 15.0356°E]) and 1 time-dependent structure function in Rijeka Bay (connected to the northern Adriatic by Kvarner Bay), all determined by data assimilation. The model domain extends directly to the northwest from this southeastern boundary to encompass the rest of the northern Adriatic. Several runs were conducted to optimize the linear friction parameter, which was set at 5×10^{-4} m/s for the runs described below.

The advantage of this model is that it seeks to find any possible solution constrained by the shallow-water equations that permit the observed tidal ellipse tilts. The model was run through 10 iterations using all 15 tidally-analyzed bottom pressure time series and all 15 tidally-analyzed, vertically-averaged current time series to determine all the structure function time series. The cost function of data-model mismatch was evaluated over the model time period of February 1 through April 4, 2003 with equal weight given to 1 cm and 1 cm/s total rms over time and station. The final solution failed to match the observed currents at VR5, but agreed well at all other sites. This means that no solution was permitted within the constraints of the discretized shallow water equations that could match VR5 tides and the tides at other sites. This result provides the strongest evidence of a compass error at VR5.

Despite the lack of any physical evidence of instrument malfunction, the tilt disagreement with three independent modeling predictions and with neighboring stations strongly suggests a compass error is present in the VR5 data. Therefore another run of the variational assimilation model was

made, excluding VR5 current data. The solution produced tidal current ellipses at VR5 that were tilted 28° clockwise on average[12] from the tilt of the observed tidal current ellipses. Based on this result, as listed in Table 7 the currents at site VR5 were all rotated by 28° clockwise to remove the inferred compass bias error.

3.10 Missing Ensembles

For some JRP ADCPs, single ensembles were taken but not recorded in the flash memory cards. These are indicated by single 30 minute time gaps in the records as opposed to the usual 15 minute time gaps and by a missing ensemble number. This occurred at SS2, SS5, SS9, CP2, VR4, and VR5. For all but SS9 the missing ensemble was associated with the start of a new binary file on the memory cards (i.e., ending of a *.000 file and start of a *.001 file) and thus the ensemble was split between files and not converted to ASCII. A DOS append of the two binary files restored these ensembles. For SS9, the loss inside a single binary file was likely caused by a slight glitch in the ADCP CPU (RDI, personal communication).

For the JRP ADCPs, missing ensembles were identified by the time jump and then an ensemble was inserted in the gap with all values (except for time) marked as bad. Thus a uniform time step was restored to the ADCP time series. This processing step was only needed for SS9.

4. ADCP FILTERED DATA

As mentioned in Section 2, the selected sampling scheme for the JRP ADCPs was to use 4 equally spaced burst ensembles to estimate current flow for the hour. Previous sections described processing of the individual burst ensembles, but further processing is needed to average and decimate the 15 minute bursts to hourly samples and thereby decrease sample noise and uncertainty.

4.1 Depth

As described in Section 3.3.3, efforts were made to keep a constant truncation depth below the moving sea-surface. Thus, certain ADCP bins near the surface have good values only during times of infrequent high sea level and are marked as bad at all other times since they fall into the surface interference zone. Such bins are not ideal for filtering and further analyses and are excluded from the final hourly data set although maintained in the 15 minute data set. For a bin level to be included in the hourly data set it was required to have less than 50% of the 15 minute velocity ensembles marked bad by the total set of quality control steps previously described. Two bins were excluded from VR4, no bins were excluded from SS9, SS10, and VR6, and one bin was excluded from the other sites.

Since the range of each ADCP bin changed negligibly over the deployment, a mean depth below sea-level was calculated for each bin as the average (over the deployment) of the optimized range of the sea surface to the ADCP head (see Section 3.3.2) minus the reported range of the bin to the ADCP head. Thus a hypothetical bin having a mean depth of zero would indicate that this bin is centered at mean sea level (over the deployment). The depths listed in Table 1 for the JRP

[12]This result is produced using either the average tilt difference from the Q_1, O_1, P_1, K_1, N_2, M_2, S_2, and K_2 constituents or the average tilt difference from the three most dominate constituents (K_1, M_2, S_2) or the median angle difference between the observational and simulated velocities.

moorings are the optimized mean depths of the sea floor from the sea surface and thus these values could be used to convert the bin depth reference from the surface to the bottom if needed.

4.2 Velocity Data

Standard filtering techniques were used to combine velocity measurements and obtain hourly values because such techniques allow the best damping of energy from frequencies above the new Nyquist frequency and preservation of energy from frequencies below the new Nyquist frequency. However, the disadvantage of this is the requirement for time series without gaps or Not a Numbers (NaNs) and thus a need for interpolation and extrapolation. Since tidal fluctuations have such strong spectral peaks, they were removed prior to filtering and then added back to the final time series. Tides were removed using the Response Method of Munk and Cartwright (1966). Since this method calculates spectral admittance, the removal of NaNs from the velocity time series must be done prior to the tidal calculations.

Method four[13] of the program inpaint_nans.m, written by John D'Errico and available from MATLAB® Central exchange, was used to replace all velocities marked as bad values with values determined by interpolation and extrapolation from neighboring times and depths. The code finds the least-squares solution to an overdetermined set of equations where every cell to be determined is set equal to its neighboring cells (before and after) in time and (above and below) in depth. Boundary cells have fewer neighbors and therefore fewer equations. The solution is equivalent to finding values for all bad cells such that their values are equal to the average of the four (or fewer) adjacent cells to these cells. Thus one step in time (15 minutes) is treated equally with one depth bin (Table 3) with respect to average weighting[14].

The main reason why this program was selected over other possible choices for interpolation and extrapolation was its behavior at the boundaries. Requiring the cells to be equal to the averages of their neighbors constrains the extrapolation behavior to values lower than the maximum value bounding the block of NaNs as it allows information and patterns from the bounding cells to "fill in" the missing values. This is especially important for the top ADCP velocities as the moving sea-surface and surface interference zone can cause the top cells to have bad values for low tides and good values for high tides. Thus the blocks of bad data are semi-periodic with periodicities at tidal frequencies. The tidal solution of the top bin is influenced by this and is sensitive to the extrapolation method that is used. inpaint_nans.m method four was found to produce the least divergent (from neighboring depths) tidal solution for this top bin.

After interpolation and extrapolation for all bad values, the Response Method was used to remove tidal fluctuations from the east/west (u) and north/south (v) ADCP velocity time series. Bad values were also filled in for vertical velocity (w) and then all three of the velocity time series were interpolated in time such that the new time base aligned exactly with 0, 15, 30, and 45 minute points of every hour. This step was done to align the time base of every JRP ADCP station with each other. The ADCPs were synchronized at the start of their measurements for these times and therefore the interpolations[15] were in practice only over half of their respective burst durations (31–41 s, see Table 3) and had a very small effect. A 2-hour low-pass, 2nd-order Butterworth filter

[13] Inside the publicly available inpaint_nans.m download package, documentation of method four is inaccurate.

[14] A consequence of this is that time and depth weighting were different for sites SS2, VR1, and VR4 with smaller depth bin sizes.

[15] linear extrapolation for the first point.

was built and the velocity time series were filtered with it run forward and backward to preserve phase. After filtering, tides were added back into the u and v time series and versions with and without tides were kept. Finally, any periods of bad data longer than 1 hour in the original velocity time series were reinstated and the velocity time series were decimated to hourly values aligned with the hour.

4.3 Velocity Error Estimates

There are two distinct types of ADCP velocity errors, (1) bias error and (2) random error (RDI, 1999). Both these sources of uncertainty affect the velocity estimates made from every acoustic measurement ping of the ADCP, but while (2) is reduced by the averaging of pings (1) is constant for all pings and will also remain unchanged with depth and time averaging. According to RDI the best estimate of ADCP velocity bias and thus long-term uncertainty is $\pm 0.5\%$ of the current magnitude plus ± 0.5 cm/s for 300 kHz ADCPs and $\pm 0.3\%$ of the current magnitude plus ± 0.3 cm/s for 600 kHz or 1200 kHz ADCPs. These and the sampling error of approximately ± 0.4 cm/s (see Section 2) arise strictly from the method of estimating the velocities and should be added to the ensemble random error estimate to determine total uncertainty.

As discussed in Section 3.5, RDI ADCPs provide an "error velocity" formed from two independent measures of vertical velocity and weighted such that its variance should be equivalent to the uncertainty (random error) of the horizontal velocity components. Thus before filtering, the random error can be estimated simply as the standard deviation of the error velocity time series at each depth level. The standard deviation is only taken over error velocities from velocities not marked bad by the data processing described throughout Section 3.

Velocity values that were filled in by interpolation (Section 4.2) should have different uncertainties than other velocities. To estimate the expected error for these, velocities at the same time but from all other depth bins were determined by linear time interpolation from their neighbors and then subtracted from the actual measured value to produce an error value. Then the extra error associated with interpolation at a given time and depth level was assigned the rms error over all other depth levels and over u and v for the same time. For rare cases when all depth levels for both u and v were interpolated at a given time, the expected errors were instead assigned to the time-average of the interpolation errors at the same depth level.

To account for error propagation through the Butterworth filter run forward and backward, we took advantage of the fact that any linear filter operation can be alternatively described by multiplication of an N by N matrix of data weights with a column vector version of the original (length N) time-series data. The relatively high cutoff frequency of our filter allowed the N by N matrix to be accurately approximated with a smaller (100 by 100) matrix. 17 weights (columns) surrounding the center (row 50, column 50) of the smaller matrix were copied for all time points[16] to fill out a sparse data weighting matrix for the actual N by N size filter. Without making this matrix sparse (by the well justified approximation that the filter only significantly draws from 17 points) the computation would be prohibitively expensive. Finally these data weights were used in normal error propagation formulas to calculate the final expected random errors for the filtered velocity time series. The average value of these for the JRP ADCP velocities is ± 1.3 cm/s.

[16] except for the first and last eight time points which were directly extracted from the first and last 17 columns of the 100 by 100 matrix.

The error velocity time series also provide an estimate of the time and depth correlations of the horizontal velocity random errors if these error correlations can be approximated as being the same as those of the vertical velocities. To investigate time correlations, a time correlation scale was calculated from the vertically averaged error velocity time series for all JRP ADCPs. All error time correlation scales were less than 17 minutes indicating that the velocity errors are essentially uncorrelated with respect to ensemble (15 minute) sampling. This agrees with the expected performance of the ADCP and the theorized nature of the random errors (RDI, personal communication). Further tests using individual depth level time series at sites SS2 and VR6 show that error time correlation scales can be higher[17] for surface bins. This could be related to the influence of non-standard environmental factors or simply be an artifact of added correlation from using interpolated values across gaps in this calculation.

The expected depth correlations for the velocity errors are 15% between adjacent bins due to a geometric overlap of depth bins (RDI, 1999) and 0% otherwise. However, for the JRP ADCPs the actual velocity error depth correlations were slightly higher than these theoretical values. These correlations were estimated by calculating correlation coefficients between all pair combinations of error velocity time series at all JRP ADCPs. Figure 12 shows an example from station SS6. The main area of correlation is between adjacent bins, but this correlation is higher than 15% in the upper water column and lower than 15% in the lower water column, and weak correlation extends over several further bins in the upper water column. There are some site to site variations in this pattern with the upper water column extension of correlation weaker or greater than the SS6 example, but all velocity error depth correlations at all stations are relatively weak and departures from theory (15% correlation only between adjacent bins) are mild.

4.4 ADCP Temperature Data

RDI ADCPs record the temperature at the ADCP head. As discussed in Section 3.1, older models locate the temperature thermistor underneath the transducer head while newer models locate it above and external to the transducer head in close contact with the water. This difference has a pronounced effect on the response of the sensor and there is significant attenuation of fluctuations at periods shorter than 17 hours (Walsh, personal communication) for the older models. Another aspect of this effect that should be considered is the adjustment time of the sensor during deployment as it changes equilibrium from the air temperature to the bottom water temperature. As discussed in Section 3.1, the ADCP temperatures were marked as bad during the determined adjustment times as these measurements were contaminated with residual surface thermal effects. The times varied from a high of 16 hours at station SS6 to a low of 1 hour at station SS2 with half of the ADCPs having adjustment times longer than 4.5 hours and half shorter.

The only additional processing steps applied to the ADCP temperature records were (1) linear interpolation to align the time base with exact 0, 15, 30, and 45 minute points and (2) use of the same 2-hour low-pass, 2nd-order Butterworth filter run forward and backward as used on the velocity records, followed by (3) decimation to hourly values aligned with the hour, as with the velocities. The temperature sensor specifications give an uncertainty of $\pm 0.4^{\circ}$C. However, no specific error variables were created for temperature to account for propagation of this uncertainty through the

[17] Error time correlation scales were below 17 minutes for these sites except for 13 hours (SS2 1.9 m depth, 45% data interpolated), 1 hour (SS2 2.4 m depth, 17% data interpolated), and 1.6 hours (VR6 2.6 depth, 43% data interpolated).

"analog filter" responsible for the attenuation of temperature fluctuations or propagation through the digital Butterworth filter.

4.5 Merging and Filtering VR1 data

Filtering data for station VR1 required slightly different procedures to allow for the fact that the measurements were divided into two different periods and that the instrument settings were different for these periods (Table 3). First, the bin depths of the two instruments were calculated according to a common reference of the mean sea level for the entire deployment. This was done by subtracting the bin range to the ADCP head from the mean of the combined (from each half) time series of optimized range of the sea surface to the ADCP head (Section 3.3.2). Then the VR1a u, v, and w data (finer depth grid) were interpolated onto the depth grid of VR1b[18] (coarser depth grid). Where interpolation required the combination of good and bad values, the good values were used unaltered. Estimates of velocity uncertainty were made for the VR1a period by taking the standard deviation of the velocity error time series from VR1a. This was regridded onto the VR1b depth levels by standard error combination formulas[19] for cells at times where actual velocity interpolation had been done and by direct copy of individual velocity error standard deviation values when velocity interpolated had not been used.

A complication in merging and filtering VR1 data is that VR1a ensembles are taken every hour rather than every 15 minutes as at VR1b and other sites. Thus filtering and decimation should not be done on the VR1a data due to its differing, long, single-burst sampling strategy. However, filtering and decimation are needed for the VR1b half and an estimate of the tides is needed to remove these fluctuations prior to filtering. To include VR1a data in the tidal estimates, new time series[20] were formed with 15 minute data spacing, where all values were filled in for VR1b times and only every fourth value for VR1a times. Other values during VR1a times were marked as bad. Then these new time series were run through the same interpolation and extrapolation and Response Method tidal analysis (Section 4.2) used at other sites. The tidal results obtained in this way were compared to results from various other techniques for estimating these tides (including harmonic methods) and found to be in good agreement.

For the VR1b half, after the detided time series were obtained, all other filtering and decimation procedures were identical to those already described for the other sites. For the VR1a half, bad velocity values were filled in only if the data gaps were single points in time (1 hour) and no further[21] processing was done. Then the two halves were merged to provide time series of u and v (with and without tides), w, temperature, and horizontal velocity error uncertainty for the entire deployment period.

5. ADCP AUXILIARY DATA

The JRP ADCPs provided several additional types of scientific data besides those already discussed in Section 4. These are pressure data at three sites, backscatter intensity data at all

[18] The top two bins were not used since they had 98% and 61% bad values for VR1b respectively.
[19] Approximating the correlations between adjacent bin velocity errors to be 15%
[20] Avoiding time interpolation, 7 seconds offset from the exact hour was ignored for VR1a and 45 seconds offset from exact 15 minute points was ignored for VR1b
[21] Depth interpolation and tide removal had already been done.

sites, and wave data for the VR1b deployment. To maintain the highest time resolution possible for these data, they were not filtered.

5.1 ADCP Pressure Data

As discussed in Section 3.3.1 and shown in Table 2, pressure was recorded by the ADCPs at sites SS4, SS10, and VR1b. These pressure records include both the effects of "water pressure" and atmospheric pressure as they record the pressure at the ADCP head. However, an unknown constant is subtracted out of the record so as to make the pressure value zero when the instrument is turned on. For consistency with the wave/tide gauge records (see Section 6.1) and to provide a clearer record, the ADCP pressure records were adjusted by a constant to set the mean of the pre-deployment, on-deck ADCP pressures equal to the mean of the atmospheric pressure time series (derived from the gas platform records, see Section 3.3.1) interpolated at the on-deck times. Thus our best estimate of the subtracted constant has been added back into the record.

The resulting pressure time series were truncated in time to include only times when the instruments were actually deployed on the bottom. The truncation times were identical to those identified for the velocity records (Section 3.1). Thus total pressure time series are provided for SS4, SS10, and VR1b.

5.2 ADCP Echo Intensity Data

The ADCP records the echo intensity in decibels from the backscattered acoustic pings for each bin and each ensemble. In addition to our utilization of this signal to track the sea surface fluctuations (Section 3.3.2), these data could be used to examine zooplankton concentration and movement in the water column, sediment suspension near the bottom, and bubble generation and penetration during storms near the surface. There is clear evidence (intensity peaks and patterns) of all these processes occurring in the JRP ADCP dataset.

Echo intensity data are provided for each of the four ADCP beams. A simple average was made to compute average echo intensity for each bin at each time. These data were then truncated in time (Section 3.1) to include only times when the instruments were on the bottom. No further processing was done. Therefore these data are not calibrated and the effects of variable ADCP transmitted power, water column absorption, and beam spreading have not been accounted for (RDI, 1999).

5.3 VR1b ADCP Wave Data

The ADCP deployed at station VR1b was equipped with the RDI waves hardware and software package. The ADCP combines measurements of orbital velocities of the waves, acoustic tracking of the sea surface, and pressure fluctuations to produce estimates of surface gravity wave parameters and spectra (RDI, 2001). These include significant wave height, peak period, peak direction, wave height spectra, and directional spectrum.

The VR1b ADCP was set up to measure waves every 6 hours using 1200 pings taken at 2 Hz (i.e., 10 minute duration wave burst). The data from these bursts were interleaved with the normal

current measurement bursts and the RDI program WavesMon[22] was required to process the data into separate currents and waves datasets. WavesMon processing used settings of 42 cm transducer altitude, 1024 fft sample length, 128 frequency bands, 90 angles, and Blackman-Harris windowing, most of which are defaults (RDI, 2001). All settings that were used are saved in the test2.sst set of configuration files. The final product is a series of wvs data files that contain all the calculated wave parameters and spectra, and can be viewed using the RDI WavesView software (RDI, 2001).

6. WAVE/TIDE GAUGE DATA

Most JRP BARNYs (see Table 2) contained a SBE 26, Sea-Bird Electronics Seagauge Wave and Tide Recorder (WTG). At stations SS2, CP2, and KB1 the WTGs were coupled with SBE 4, Sea-Bird Electronics Conductivity Sensors. Complete descriptions of these instruments are beyond the scope of this report. However, complete details for the WTG are provided in the SBE 26 Operating Manual, referenced here as SBE (2000). A specification page for the SBE 4 cell can also be obtained from Sea-Bird Electronics.

WTGs store collected data in a hexadecimal format with wave and tide information interleaved. Sea-Bird software, Seasoft for Waves, can both download these data and decode them into an ASCII format. However, this program produces a time stamp by simply reading a recorded start time and applying the planned time step uniformly for each record that it reads. This is acceptable as long as the original storage or the download of the hexadecimal data does not skip any records. If a record is somehow lost before decoding, then the next record in the series is assigned the time of the missing record. This has occurred both for projects prior to and after ACE, leading to significant errors in the time records of data decoded by Seasoft for Waves. Therefore custom code was written by J. W. Book to decode the hexadecimal data while carefully monitoring the wave burst time stamps that are interleaved in the record. This code can thereby detect missing records and ensure time stamp accuracy to within the frequency of programmed wave bursts. However, for the JRP WTG, there were no missing hexadecimal lines and either the custom code or Seasoft for Waves can be used to correctly decode the data. For redundancy both were used and the results compared, but the outputs of the custom code are used as the definitive dataset. Each WTG data type is discussed below.

6.1 WTG Pressure Data

The main WTG measurements are long-term pressure time series from Paroscientific Digiquartz pressure sensors. These sensors provide continuous averaging of pressure over a programmable interval (SBE, 2000). The pressure integration interval was set to 20 minutes for the JRP WTGs. The original time stamp assigned to the pressure gauge record gives the time of the start of the pressure integration (SBE, 2000). However, using the start time for each time-averaged sample in further analysis can be confusing and/or lead to phase errors (e.g., tidal analysis). Therefore the time stamps of the integrated pressure data are shifted such that the new times are at the center time of each pressure integration.

Each WTG has a set pressure measurement range which impacts its accuracy. For the JRP moorings, sites SS2, SS5, CP2, KB1, and VR2 had 200 pounds per square inch absolute (psia) full scale ranges, sites CP3, VR4, VR5, and VR6 had 300 psia full scale ranges, and sites SS6, SS8, and

[22] Version 2.01

SS9 had 400 psia full scale ranges. The absolute accuracy of the WTG is 0.01% of these full scale ranges (SBE, 2000), i.e., ±1.4 mbar, ±2.1 mbar, and ±2.8 mbar respectively for the 200, 300, and 400 psia ranges. Based on the JRP 20 minute integration time, the expected random error in the integrated pressure time series is ±0.004 mbar, ±0.007 mbar, and ±0.009 mbar for the 200, 300, and 400 psia ranges respectively (SBE, 2000), which at most impacts only the final reported ASCII digit.

Truncations of the WTG data were done to exclude data from periods where the BARNY was not on the bottom. The BARNY deployment release time was used to establish the start of stable bottom time and the a time of two minutes prior to the BARNY main housing appearing at the surface was used as the end of stable bottom time. This latter time includes a rough estimate of the time required to winch the BARNYs to the surface, but in any case truncation points were each carefully checked against the pressure data itself to help ensure that all records contaminated by BARNY deployment and recovery were eliminated. The data records include a column of "bad data" flags. Some of these are marked with a value of one, but these flags in all cases refer to temperature and/or salinity problems (see Sections 6.2 and 6.3) rather than pressure problems. There are no indications that any of the pressure values in the data files are bad. Atmospheric pressure fluctuations were not removed from these data.

6.2 WTG Temperature Data

The WTGs take temperature measurements in addition to the standard integrated pressure measurements. A temperature value is reported for each pressure value, but the temperature value is not integrated like the pressure. The temperature represents the measured value at the end of the pressure integration period (SBE, personal communication). Therefore since the time stamp in the data file refers to the center of the pressure integration, a further 10 minutes should be added to this time when using these temperature data. The Sea-Bird specified accuracy of the temperature sensor is ±0.02°C with a random error level of ±0.01°C (SBE, 2000).

The same temperature equilibrium problems that occur for the ADCP temperature sensors inside the transducer head also occur for the WTG temperature sensors. I.e., there is significant attenuation of fluctuations at periods shorter than 17 hours in WTG temperatures (Walsh, personal communication). Also the WTG temperature sensors take some time to adjust to bottom temperatures after BARNY deployment. As was done for the ADCP temperatures, the equilibrium adjustment time was estimated by visual examination to find the first point where temperature change stabilized or switched directions after deployment. However, unlike the ADCP temperatures during the equilibrium adjustment, these WTG temperatures were not changed to NaN. Instead, the "bad data" flags for these rows were flagged with ones indicating unreliable temperature data. The estimated equilibrium time varied from a low of 2 hours 40 minutes to a high of 10 hours 20 minutes. Exactly half of the equilibrium times were 5 hours or longer.

6.3 WTG Salinity Data

As mentioned in Section 6, WTGs at sites SS2, CP2, and KB1 were equipped with SBE 4 conductivity sensors. Conductivity is recorded at the same time as WTG temperature and therefore the times for the WTG conductivity and salinity should also be lagged 10 minutes from the pressure times. The typical drift of the conductivity sensor is ±0.0003 Siemens/m per month (SBE,

2000) which translates to ±0.003 psu per month[23]. SBE (2000) specify the random error level as ±0.00002 Siemens/m (±0.0002 psu). However since the conductivity sensors are inside BARNYs where outside flow is restricted, it is anticipated that fluctuations at periods faster than 17 hours will be attenuated. In fact, comparisons of WTG conductivity and temperature records show little lag between the time series (Walsh, personal communication) suggesting that frequency attenuation should be similar. However, unlike for temperature, comparisons between simultaneous conductivity measurements internal and external to a BARNY have not been done. Also any possible effect on salinity of differing frequency responses of the temperature and conductivity sensors inside a BARNY has not been studied.

The time required for equilibrium to be established after deployment should be as long or longer for salinity as for temperature. Therefore the salinity values for the temperatures flagged as bad data should also be treated as bad, and it is possible that salinity contamination continues for a few samples beyond the period of temperature contamination. In addition to the brief periods of bad salinity data at the start of each record, the record at site CP2 shows signs of bad salinity values due to biofouling on three occasions. On December 6 and on December 12, conductivity and salinity values suddenly drop by 2 psu or more, stay at these lower salinities for a few points, and then suddenly return to their previous values. On December 9–10 the pattern is less clearly caused by biofouling, but the sudden salinity drops and rises are still suggestive. The entire period was one of strong bora winds and station CP2 is located relatively close to the Po River, so there is some possibility that these salinity drops are real. However, because the temperature/salinity characteristics of these measurements were not observed at other times, it is likely that these data are bad and therefore they were flagged as such. There were no indications of biofouling problems at either station SS2 or KB1.

6.4 WTG Wave Burst Data

A secondary measurement of the WTGs was a periodic recording of high-frequency bursts of pressure data to characterize surface gravity waves. The JRP WTGs were programmed to record 300 pressure samples at 2 Hz every 6 hours. The expected random error in the wave burst pressure values is ±0.09 mbar, ±0.13 mbar, and ±0.18 mbar for the 200, 300, and 400 psia ranges respectively (SBE, 2000). The number of digits output to ASCII[24] for the wave burst data does not reflect the number of significant figures of the measurement. Truncation of the WTG wave burst data to exclude data from periods when the BARNY was not on the bottom was done in a similar manner to the truncation of the integrated pressure data. No further processing of these data was done. With proper analysis, surface gravity wave properties can be determined from these data, although accuracy of the properties will be greatly influenced by the mooring depth because of surface gravity wave pressure attenuation with depth.

7. DATA DVD

A DVD containing the JRP winter 2002/2003 mooring data accompanies this report. Both processed and raw forms of data are provided. Detailed descriptions of the data format can be found on the DVD. All data processing was redone prior to the release of this report and DVD.

[23]Based on a conductivity of 4.1 Siemens/m, a temperature of 10°C, and a pressure of 50 dbar (approximate salinity of 37.98 psu)

[24]chosen to match Seasoft for Waves

The mooring data on the DVD are nearly identical to the data posted to http://radlab.soest.hawaii.edu/adria/ prior to 2007. Improvements in the DVD version mainly relate to minor corrections of WTG processing and VR1 ADCP data. The previous version was missing VR1b w values and had VR1a u and v datasets with interpolation through all data gaps instead of only those of 1 hour duration. WTG data in the previous version was processed using an earlier version of the custom written, hexadecimal decoder that contained some inaccuracies. Corrections to individual WTG data values are no more than 0.02 dbar in pressure, 0.001°C in temperature, and 0.003 psu in salinity. Corresponding changes to ADCP data from determinations of ADCP vertical range are slight as WTG pressure corrections are primarily to the means which are ignored during optimization. Single missing ensembles for SS2, SS5, CP2, VR4, and VR5 are restored in the DVD version (see Section 3.10).

8. ACKNOWLEDGMENTS

We thank the captains and crew of R/V Alliance during the adria02 and adria03 experiments for making collection of these data possible. Specifically we acknowledge the wonderful work of the NRL and NURC technical BARNY teams composed of Mark Hulbert and Ray Burge of NRL and Richard Stoner, Alessandro Brogini, and Alessandro Carta of NURC. We thank the RD Instruments technical team for their help with many detailed questions. Also we thank the Sea-Bird Electronics technical team for their help with wave/tide gauge questions. The entire adria23 working group contributed to the success of the experiments. This work was supported by the NRL Advanced Graduate Research Program and the Office of Naval Research under Program Element Number 0602435N.

9. REFERENCES

Book, J.W., H.T. Perkins, L. Cavaleri, J.D. Doyle, and J.D. Pullen, 2005: ADCP observations of the western Adriatic slope current during winter 2001. *Progress in Oceanography*, Vol. 66, 270–286.

Griffin, D.A., and K.R. Thompson, 1996: The adjoint method of data assimilation used operationally for shelf circulation. *Journal of Geophysical Research*, Vol. 101(C2), 3457–3477.

Janeković, I., and M. Kuzmić, 2005: Numerical simulation of the Adriatic Sea principal tidal constituents. *Annales Geophysicae*, Vol. 23, 3207–3218.

Lee, C.M., F. Askari, J. Book, S. Carniel, B. Cushman-Roisin, C. Dorman, J. Doyle, P. Flament, C.K. Harris, B.H. Jones, M. Kuzmić, P. Martin, A. Ogston, M. Orlić, H. Perkins, P.-M. Poulain, J. Pullen, A. Russo, C. Sherwood, R.P. Signell, and D.T. Detweiler, 2005: Northern Adriatic response to a wintertime bora wind event. *EOS Transactions*, Vol. 86, No. 16, 19 April.

Martin, P.J., J.W. Book, and J.D. Doyle, 2006: Simulation of the northern Adriatic circulation during winter 2003. *Journal of Geophysical Research*, Vol. 111(C03S12), doi:10.1029/2006JC003511, [printed 112(C3), 2007].

Munk, W.H. and D.E. Cartwright, 1966: Tidal spectroscopy and prediction. *Philosophical Transactions of the Royal Society of London*, Ser. A, Vol. 259, 533–581.

Plimpton, P.E., H.P. Freitag, and M.J. McPhaden, 2000: Correcting moored ADCP data for fish-bias errors at 0°, 110°W and 0°, 140°W from 1993 to 1995. NOAA Tech. Memo. OAR PMEL-117, 35 pp.

RD Instruments, 1999: Workhorse Documentation Help. Help file version 1.0 (Feb. 26, 1999), Teledyne RD Instruments, 14020 Stowe Dr., Poway, CA, 92064.

RD Instruments, 2001: Waves User's Guide. P/N 957-6148-00 (April 2001), Teledyne RD Instruments, 14020 Stowe Dr., Poway, CA, 92064.

Sea-Bird Electronics, 2000: SBE 26 Seagauge Wave and Tide Recorder Operating Manual. 22 Sep. 2000, Sea-Bird Electronics, Inc., 1808 136th Place NE, Bellevue, WA, 98005.

Table 1 — Locations and depths of ACE/JRP moorings. Depths are found by optimization of pressure records with acoustic tracking of the sea-surface.

Mooring	Responsible Institution	Latitude	Longitude	Depth (m)
SS2	NRL	43.83513°N	13.30660°E	24.89
SS4	NURC	43.88355°N	13.36667°E	45.52
SS5	NRL	43.93067°N	13.42610°E	56.99
SS6	NRL	43.99562°N	13.50438°E	65.90
SS8	NRL	44.25672°N	13.90525°E	64.57
SS9	NRL	44.41022°N	14.17478°E	58.88
SS10	NURC	44.48123°N	14.29040°E	51.38
CP2	NRL	44.46100°N	12.85512°E	41.86
CP3	NRL	44.54018°N	13.12453°E	41.87
KB1	NRL	44.75067°N	14.02125°E	48.34
VR1	NURC/NRL	45.31393°N	12.50814°E	16.67
VR2	NRL	45.27892°N	12.63697°E	24.92
VR4	NRL	45.18778°N	13.02810°E	32.54
VR5	NRL	45.12493°N	13.28367°E	34.71
VR6	NRL	45.05807°N	13.53603°E	33.05

Table 2 — Instrumentation for ACE/JRP moorings and deployment and measurement times. Instrumentation codes are: A = ADCP velocity and temperature, AW = ADCP waves, AP = ADCP pressure, T = wave/tide gauge pressure, waves, and temperature, S = conductivity sensor salinity. Start times are all in 2002. Stop times are all in 2003 except for VR1a in 2002.

Mooring	Instrumentation Codes	Measurement Start	ADCP Measurement Stop	Wave/Tide Gauge Stop
SS2	A, T, S	Sep. 22	May 5	May 5
SS4	A, AP	Sep. 22	Apr. 5	–
SS5	A, T	Sep. 22	May 5	May 5
SS6	A, T	Sep. 22	May 5	May 5
SS8	A, T	Sep. 22	May 6	May 6
SS9	A, T	Sep. 22	May 6	May 6
SS10	A, AP	Sep. 22	May 6	–
CP2	A, T, S	Sep. 23	Apr. 28	Apr. 29
CP3	A, T	Sep. 23	May 4	May 4
KB1	A, T, S	Sep. 22	May 5	May 5
VR1a	A	Sep. 4	Dec. 18	–
VR1b	A, AP, AW	Dec. 18	Jun. 4	–
VR2	A, T	Oct. 8	May 4	May 4
VR4	A, T	Sep. 24	Apr. 29	May 4
VR5	A, T	Sep. 24	May 4	May 4
VR6	A, T	Sep. 24	May 4	May 4

Table 3 — Settings for the ACE/JRP ADCP instruments and data. All instruments used burst sampling at 15 minute intervals and 1 Hz ping sampling frequency, except for VR1a which used burst sampling at hourly intervals and 0.5 Hz ping sampling frequency.

Mooring	Serial Number	Frequency (kHz)	Bin Size (m)	Burst Duration (s)	RDI Theoretical σ for u or v (cm/s)	Err. Velocity Threshold (cm/s)
SS2	1551	600	0.5	82	2.14	6
SS4	683	300	1.0	74	2.25	7
SS5	64	300	1.0	62	2.45	9
SS6	119	300	1.0	62	2.45	10
SS8	121	300	1.0	62	2.45	12
SS9	123	300	1.0	62	2.45	10
SS10	1204	300	1.0	74	2.25	10
CP2	1461	300	1.0	74	2.25	8
CP3	122	300	1.0	74	2.25	9
KB1	699	300	1.0	74	2.25	8
VR1a	228	1200	0.35	960	0.94	5
VR1b	1568	1200	0.5	90	1.21	5
VR2	116	300	1.0	82	2.13	6
VR4	1535	600	0.5	82	2.14	8
VR5	98	300	1.0	82	2.13	10
VR6	117	300	1.0	82	2.13	10

Table 4 — The means and their difference in meters of the range to the sea surface (from the ADCP transducer head) time series derived from pressure and acoustics respectively. The pressure measurements were made by wave/tide gauges in the moorings or pressure sensors in the ADCP and were converted to depths by the methods described in Section 3.3.1. The acoustic measurements were calculated from the echo intensity data with a resolution of the ADCP bin size.

Mooring	Mean Pressure derived Range	Mean Acoustics derived Range	Difference of Means
SS2	24.48	24.30	0.18
SS4	45.34	44.88	0.46
SS5	56.84	56.30	0.55
SS6	65.83	65.20	0.63
SS8	64.29	63.76	0.53
SS9	58.53	58.10	0.43
CP2	41.55	41.10	0.45
CP3	41.57	41.10	0.46
VR1b	16.38	16.24	0.14
VR2	24.61	24.25	0.36
VR5	34.51	33.89	0.61
VR6	32.84	32.34	0.50

Table 5 — Comparison of various methods of measuring the total water column depth (in m) at the time of ADCP deployment. The measurements from the ship were done with the ship's echo sounder and recorded at the time of release of the deployment tackle from the mooring. The pressure measurements were made by wave/tide gauges in the moorings or pressure sensors in the ADCP and were converted to depths by the methods described in Section 3.3.1 except using measured densities. The acoustic measurements were calculated from the echo intensity data from the first ADCP measurement made after the deployment tackle release. *A* indicates that pressure was measured by the ADCP and not by wave/tide gauge. *B* indicates true optimization could not be performed because either the acoustic- or pressure-derived depth time series were not available. *C* indicates the lack of sound speed corrections for acoustics and the lack of measured densities for pressure because hydrographic data were not taken at deployment.

Mooring	Ship S	Pressure P	ADCP Acoustics A	Optimized O	S - P	O - P
SS2	25.4	24.90	24.93	24.79	0.50	-0.11
SS4	45.3	45.91^{A}	45.26	45.55	-0.61^{A}	-0.36^{A}
SS5	57.2	57.43	57.64	57.09	-0.23	-0.34
SS6	66.3	66.51	67.04	66.13	-0.21	-0.37
SS8	64.7	64.95	66.17	64.81	-0.25	-0.15
SS9	58.5	59.13	59.64	59.01	-0.63	-0.12
SS10	51.1	51.66^{A}	–	51.41^{B}	-0.56^{A}	-0.25^{B}
CP2	42.6	42.50	42.16	42.30	0.10	-0.20
CP3	42.0	42.33	42.46	42.08	-0.33	-0.24
KB1	48.0	48.70	–	48.45^{B}	-0.70	-0.25^{B}
VR1a	–	–	16.65^{C}	16.65^{B}	–	–
VR1b	–	16.72^{AC}	16.46^{C}	16.56	–	-0.16^{AC}
VR2	25.0	24.52^{C}	24.50^{C}	24.34	0.48^{C}	-0.19^{C}
VR4	33.0	33.03	–	32.78^{B}	-0.03	-0.25^{B}
VR5	34.9	34.98	34.39	34.67	-0.08	-0.31
VR6	33.2	33.22	32.43	32.92	-0.02	-0.30

Table 6 — Trawl strikes and anomalies found in the ADCP compass data.

Mooring	# Trawl Strikes	Max Trawl Rot. (deg. CW)	Drift Inflection	Other Events (deg. CW)
SS2	4[a]	23.28	Nov. 21	Nov. 13, shifts of 0.29, -0.27, -0.20
SS4	11	-5.77	Dec. 22	Dec. 19, change in noise and drift
SS5	4	0.44	–	pitch & roll extra shifts
SS6	1	10.30	–	Nov. 18, some movement
SS8	0	–	Sep. 30, Mar. 28	none
SS9	1	1.26	–	Nov. 16, 0.31; Apr. 22&23, pitch & roll
SS10	3	-3.44	Dec. 15	Nov. 16 shift of -0.5 pitch, 0.8 roll
CP2	2[a]	0.32	–	pitch & roll extra shifts
CP3	1	6.68	–	none
KB1	0	–	–	none
VR1a	NA	NA	–	Sep. 9, 5.34; Oct. 22; Nov. 16, 6.31
VR1b	NA	NA	–	Jan. 7 shift of 1.0 pitch, -1.2 roll
VR2	0	–	Nov. 24	Nov. 16, 0.23 & -0.57; Nov. 22, pitch & roll
VR4	5	8.83	–	Oct. 2&3 shifts in pitch & roll
VR5	0	–	Nov. 29, Feb. 18	none
VR6	1	-0.49	–	Nov. 16, shift of -0.26

[a] one of these identified by inspection

Table 7 — Directional corrections for the ACE/JRP ADCP instruments based on inferred compass bias and drift.

Mooring	Magnetic Corr. (deg. CW)	Total Compass Drift Corr. (deg. CW)	Tidal Model Bias Corr. (deg. CW)
SS2	1.72	-1.04	none
SS4	1.73	-1.65	none
SS5	1.75	none	none
SS6	1.76	3.96	none
SS8	1.86	3.26	none
SS9	1.92	none	none
SS10	1.95	-1.11	none
CP2	1.63	-4.40	none
CP3	1.69	2.89	none
KB1	1.89	none	none
VR1a	1.56	none	none
VR1b	1.56	2.56	none
VR2	1.59	1.17	none
VR4	1.68	none	none
VR5	1.74	1.00	28
VR6	1.79	none	none

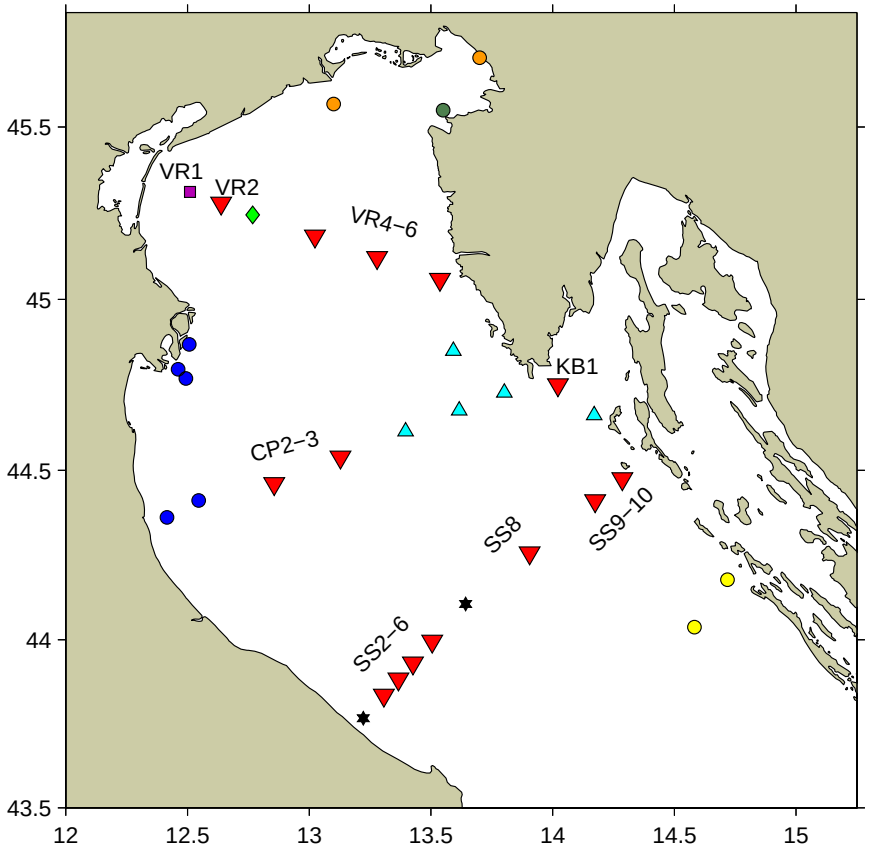

Fig. 1 — Locations of moorings deployed in the northern Adriatic during the winter of 2002/2003. Red triangles are BARNY moorings deployed by NRL and NURC. The purple square indicates the location of a JRP ADCP at the Acqua Alta Tower of the Institute for the Study of the Dynamics of Great Masses (Italy). The yellow circles are BARNY moorings deployed by the University of Zagreb, Institute of Oceanography and Fisheries, and Croatian Hydrographic Institute (Croatia). The light blue triangles are BARNY and rotary current meters deployed by the Rudjer Bošković Institute (Croatia). The dark blue circles are EuroSTRATAFORM moorings. The black stars are rotary current meters deployed by the Marine Fisheries Research Institute (Italy). The green diamond indicates a rotary current meter mooring deployed by the Institute of Marine Biology (Italy). The orange circles are moorings deployed by the National Institute of Oceanography and Experimental Geophysics (Italy). The green circle is a mooring deployed by the National Institute of Biology (Slovenia).

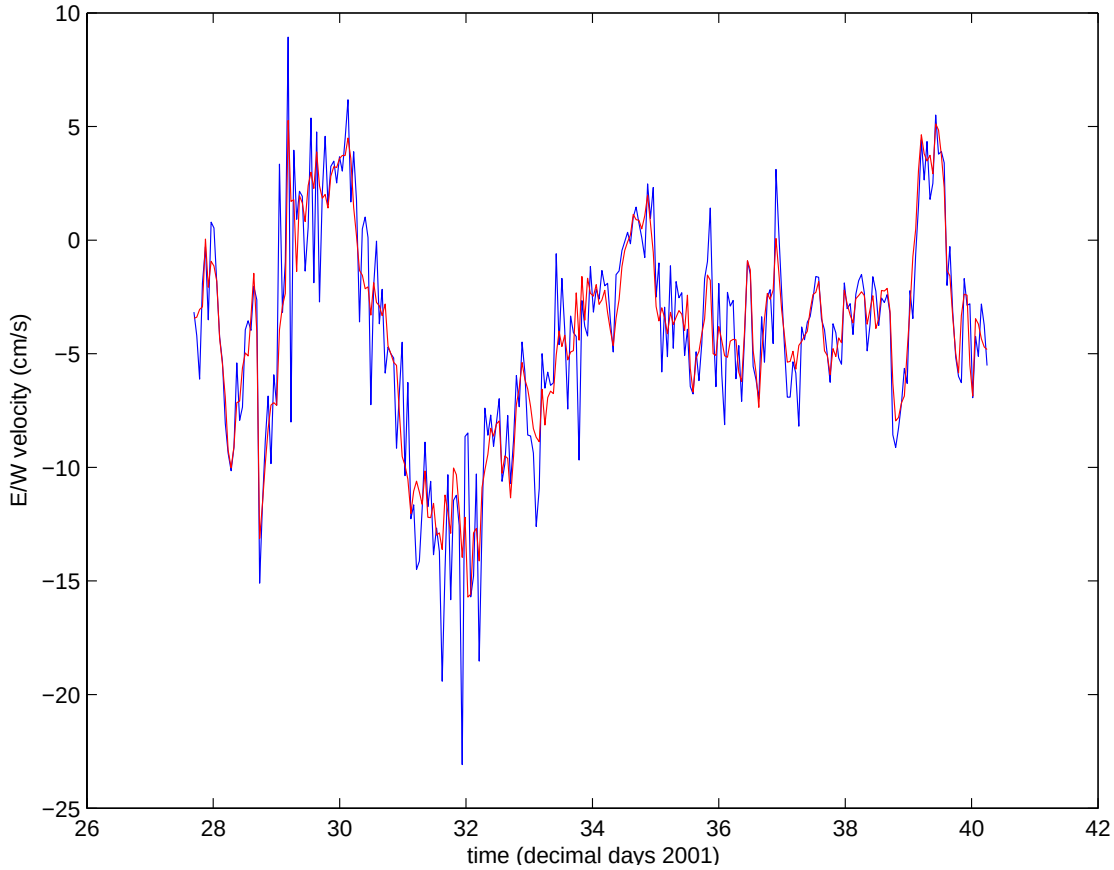

Fig. 2 — Comparison of two hypothetical sampling schemes constructed from an ADCP measured velocity time series (GMT) from 33 m depth at site SS6 during 2001. The blue line is 65 minute sub-samples of 5 minute spread-sample means used to approximate a sampling scheme of burst pinging for 5 minutes every hour. The red line is 65 minute averages of the 5 minute spread-sample means to approximate a sampling scheme of spread sampling for an hour.

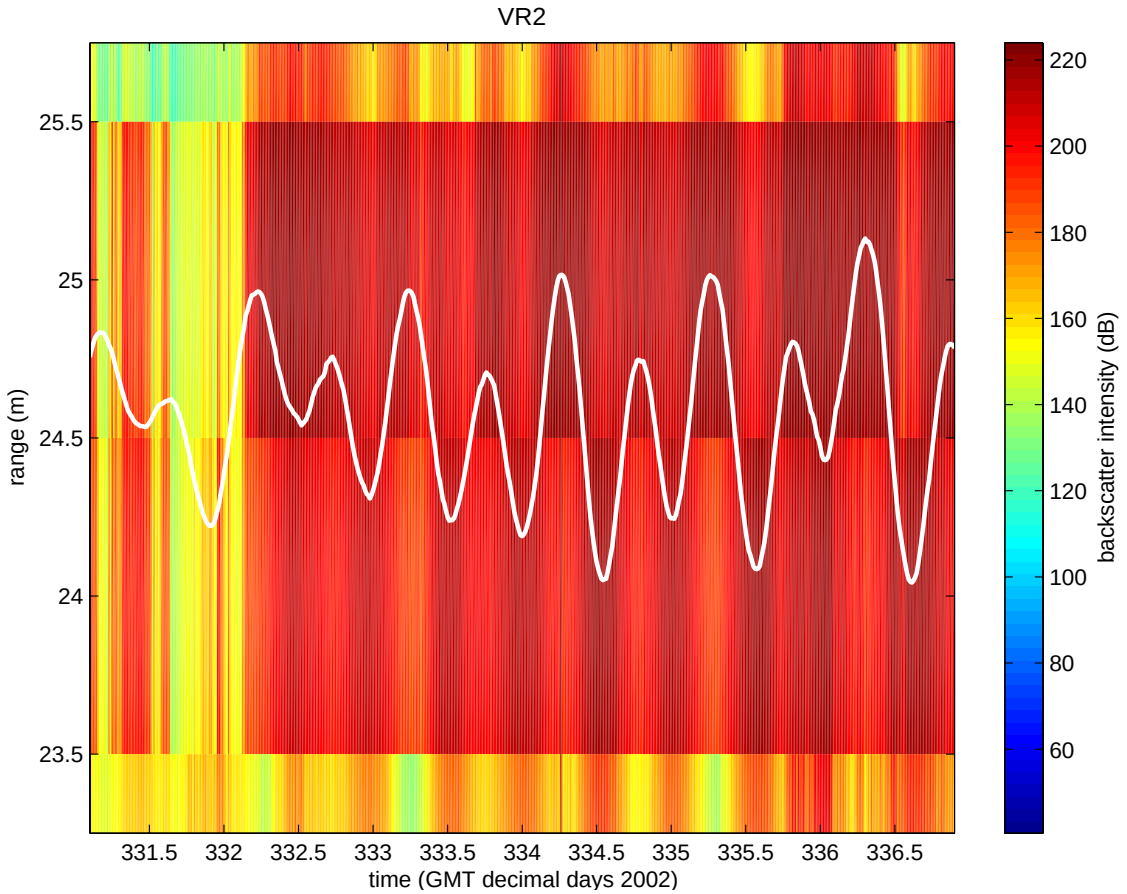

Fig. 3 — Comparison between the optimally adjusted pressure derived range to the surface and the ADCP backscatter intensity data. The colors indicate the average backscatter intensity (dB) of the four ADCP beams from mooring VR2. Only a small subset of these data is shown. The white trace is the pressure-derived, ADCP range to the sea-surface time series adjusted by a constant offset for best agreement in a least-squares sense with the acoustic backscatter data. The switching between dark and light red intensities is nicely tracked by the optimized pressure-derived time series.

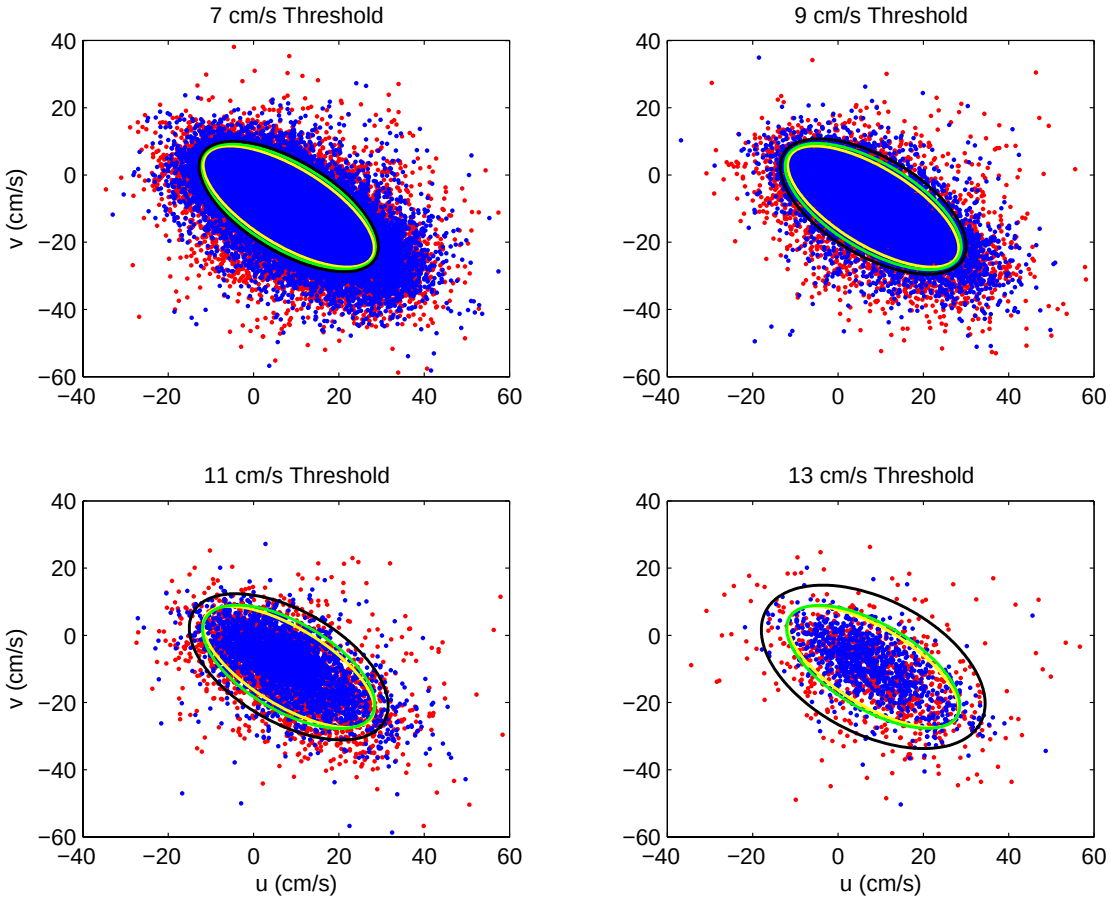

Fig. 4 — Select velocity scatter plots and std ellipses at SS5. The red dots in each panel are all velocities with an error velocity magnitude between the threshold for that panel and 1 cm/s less. The over-plotted blue dots have the same number of dots as the red set and are a random subset from those velocities with error velocity magnitudes less than 5 cm/s. The yellow 2-std ellipse is from the estimated ocean signal variance. The green 2-std ellipse is from the blue dots and the black 2-std ellipse is from the red dots. Black ellipse divergence from the green ellipse indicates the presence of additional noise for that particular error velocity band.

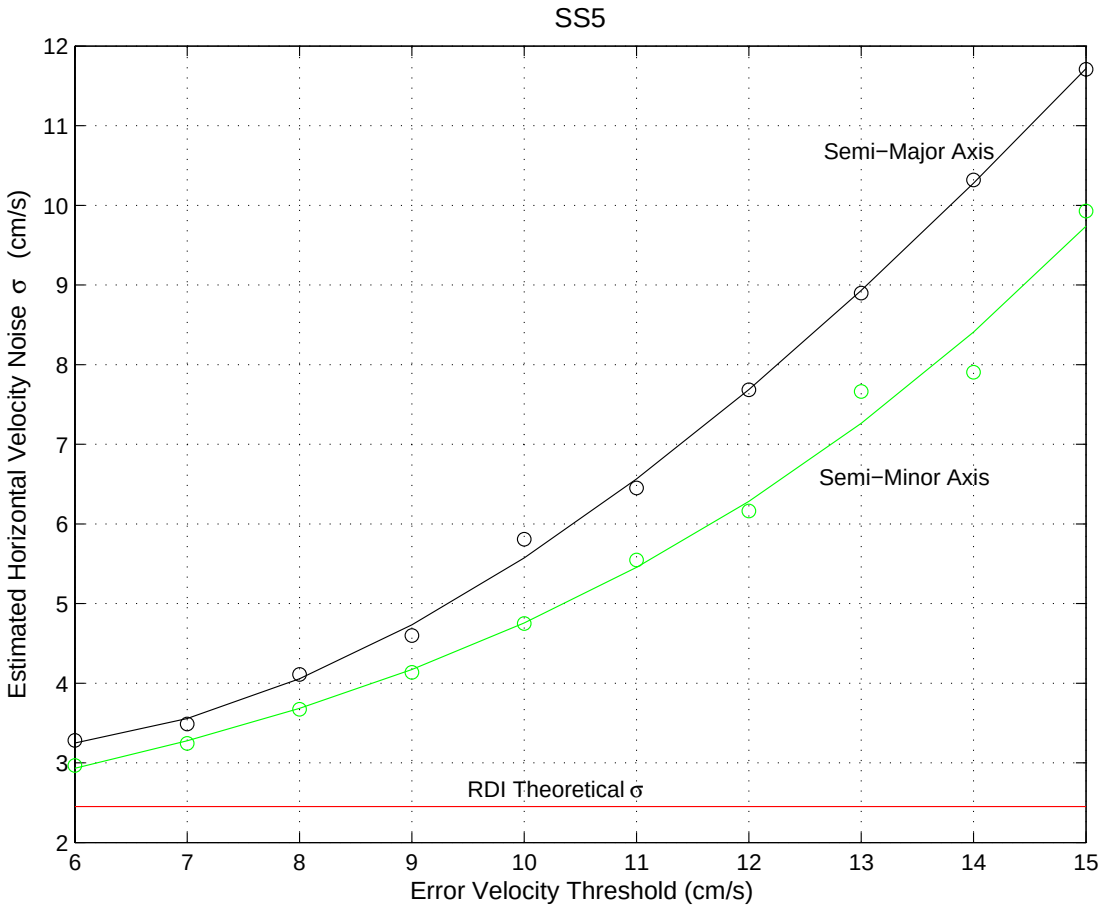

Fig. 5 — Estimated horizontal velocity noise σ in cm/s for different error velocity bands. The black circles are noise variance in the direction of the semi-major axis of current variation and the green circles are noise variance in the direction of the semi-minor axis. The lines are cubic polynomial fits to the circles. The red line marks the level of horizontal noise variance predicted for this ADCP based on its setup.

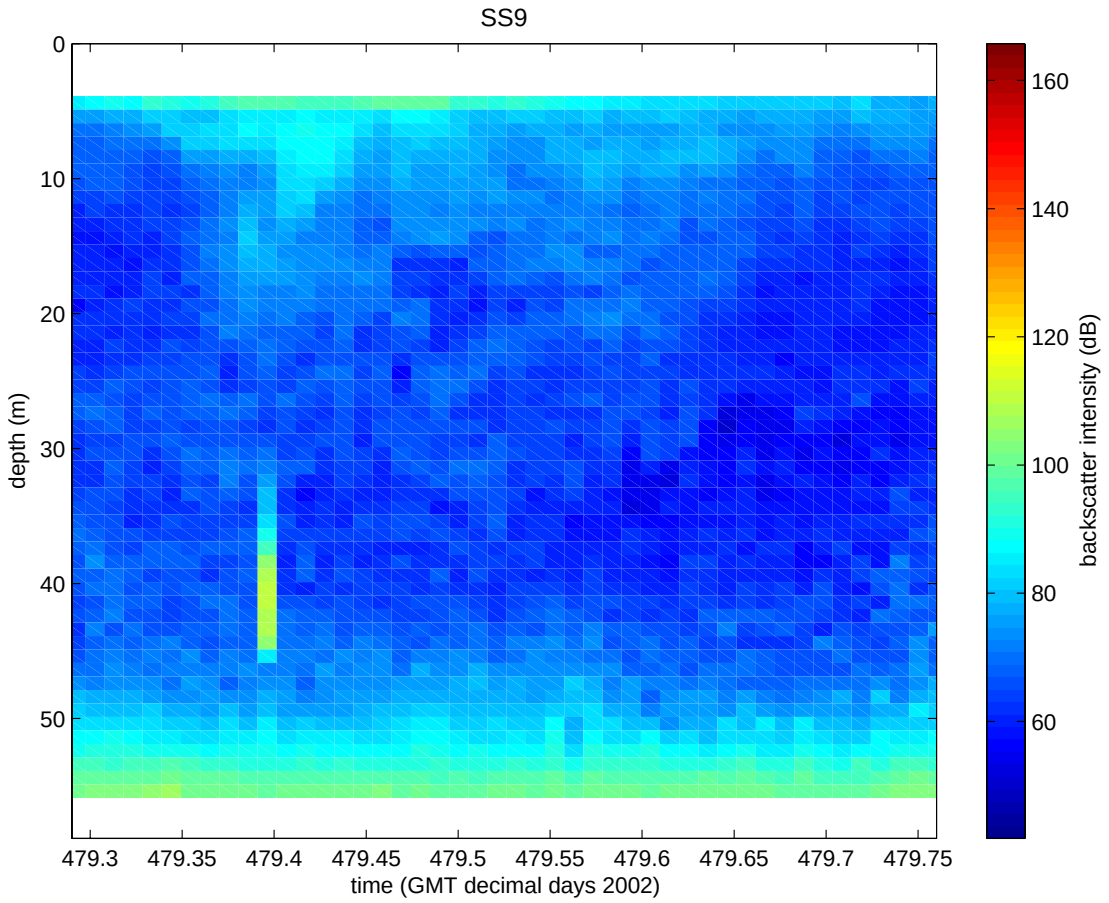

Fig. 6 — Example from mooring SS9 of a spike in backscatter intensity likely caused by fish school contamination. The colors are the average backscatter intensity (dB) of the four ADCP beams. Only a small subset of data is shown. The "fishy" spike occurs just before time 479.4 (April 25) at 40 m and extends in depth by 9 m. Such spikes are often associated with (false) velocity spikes.

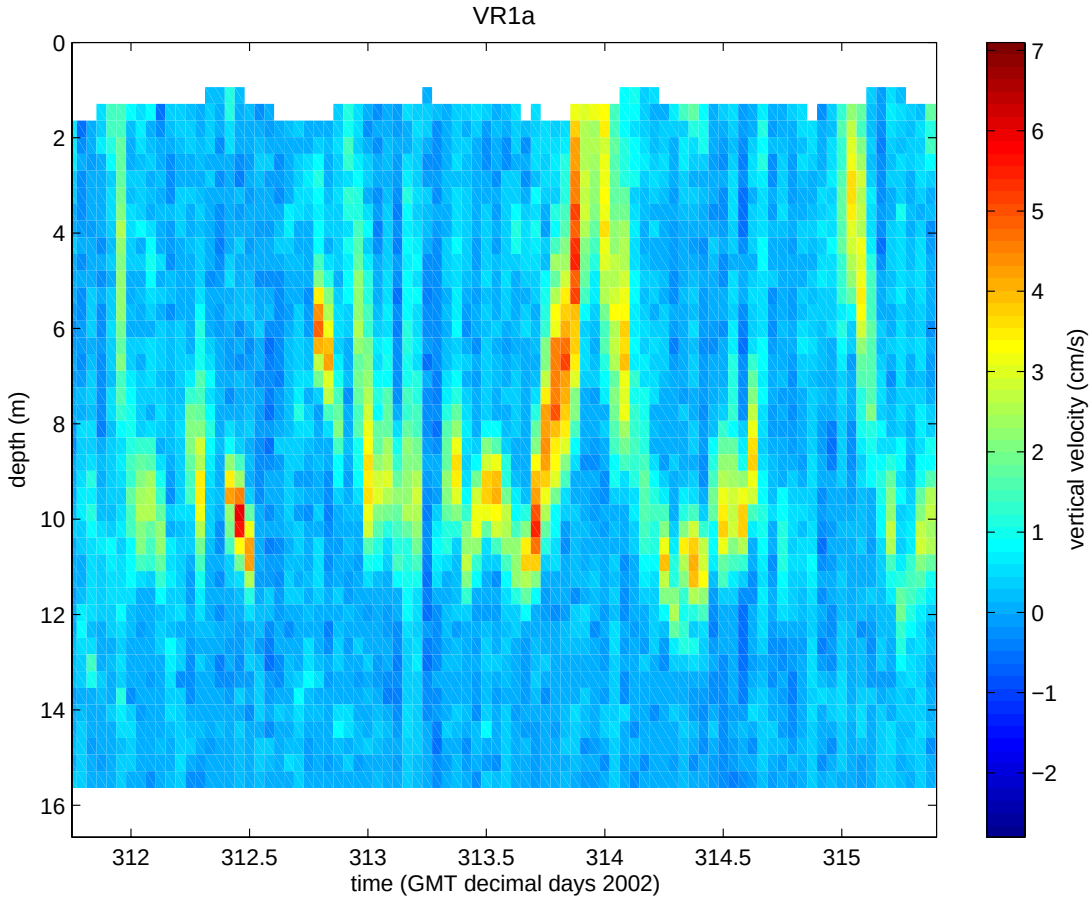

Fig. 7 — Example from record VR1a of the strong velocity contamination present throughout the VR1 ADCP data. The colors are the measured vertical velocity. Only a small subset of data is shown. Contamination can most clearly be identified as strong peaks in positive vertical velocity. These peaks are usually associated with high magnitude error velocity values and unusual patterns in horizontal velocity values. The patterns in depth and time of the vertical velocity peaks suggest that they are caused by contamination from some type of mobile biology. The high prevalence of contamination at site VR1 could be due to the presence of the nearby Acqua Alta Tower structure or the fact that the internal ADCP fish detection algorithm was disabled for these instruments.

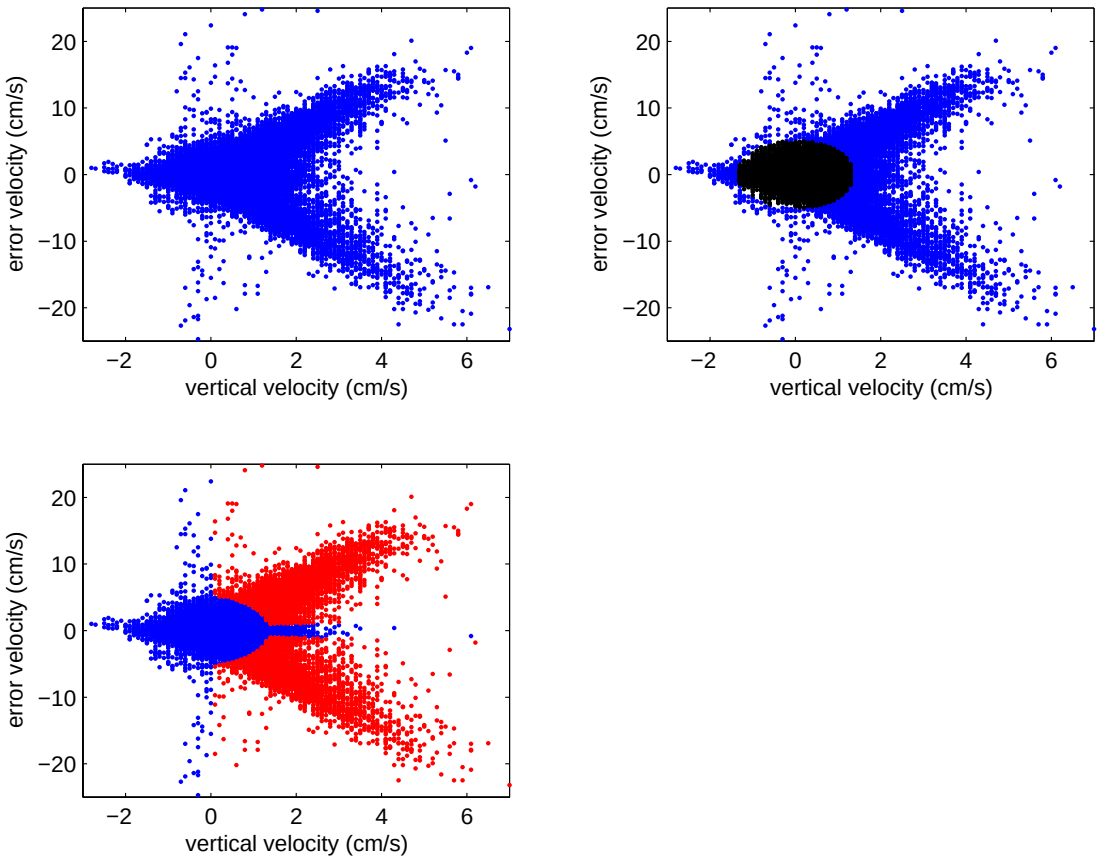

Fig. 8 — Graphical illustration of the objective procedure for detecting and removing fish contamination at VR1. The upper-left panel shows the relationship between vertical velocity and error velocity for VR1a. All positive vertical velocity ensembles were temporarily discarded from the vertical velocity and error velocity datasets. Then the remaining data were duplicated and reflected across the line of zero vertical velocity to produce a new symmetric, synthetic dataset (not shown). Standard-deviation ellipse parameters were calculated from this dataset and ensembles from the original dataset were considered uncontaminated if they fell inside the four-standard-deviation ellipse. The upper-right panel shows the VR1a dataset with black points marking the ensembles inside this particular ellipse of the reflected dataset. Finally, points outside the ellipse are considered contaminated if they have positive vertical velocities and their error velocity magnitudes exceed 1 cm/s. The bottom-left panel shows the VR1a dataset with red points marking the ensembles identified as being contaminated and therefore excluded.

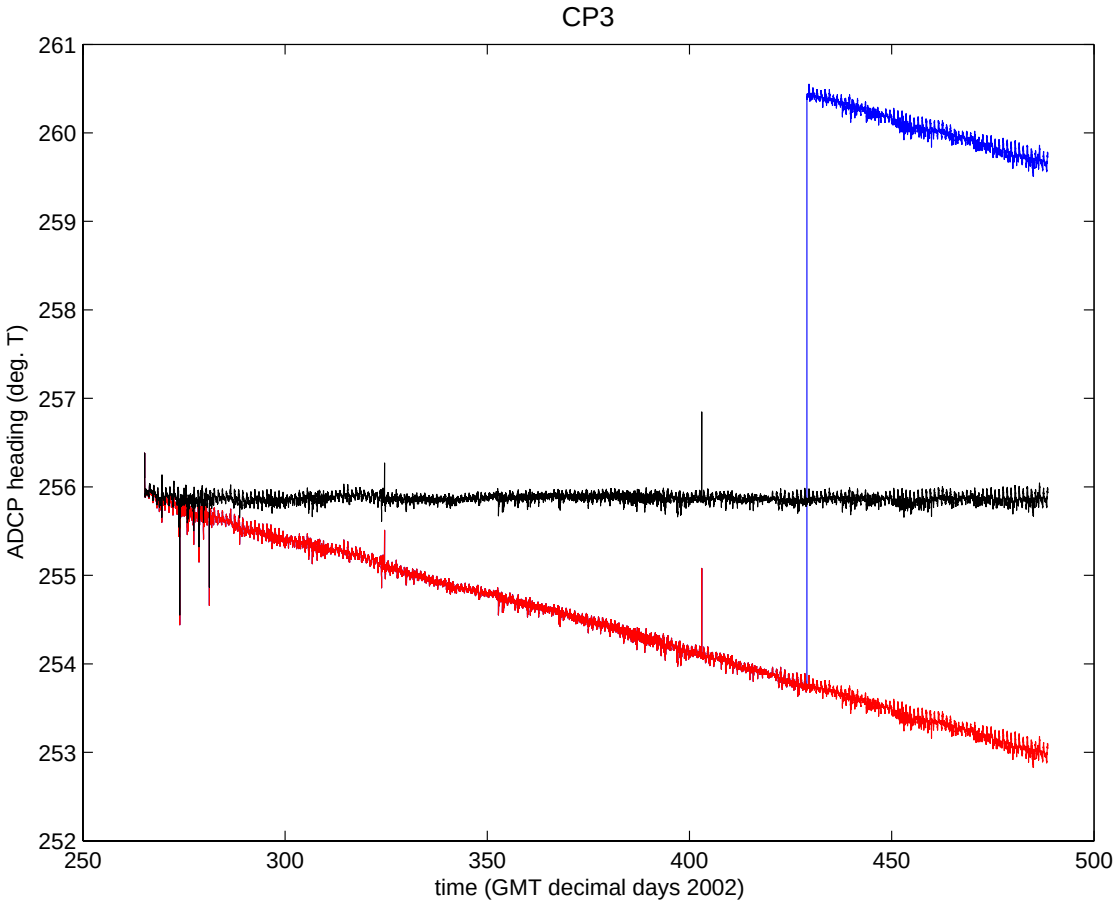

Fig. 9 — CP3 heading showing the effects of a trawl strike and linear compass drift. The blue trace is the measured heading, the over-plotted red trace is the heading with the trawl strike removed, and the over-plotted black trace is the heading with both the trawl strike and drift removed.

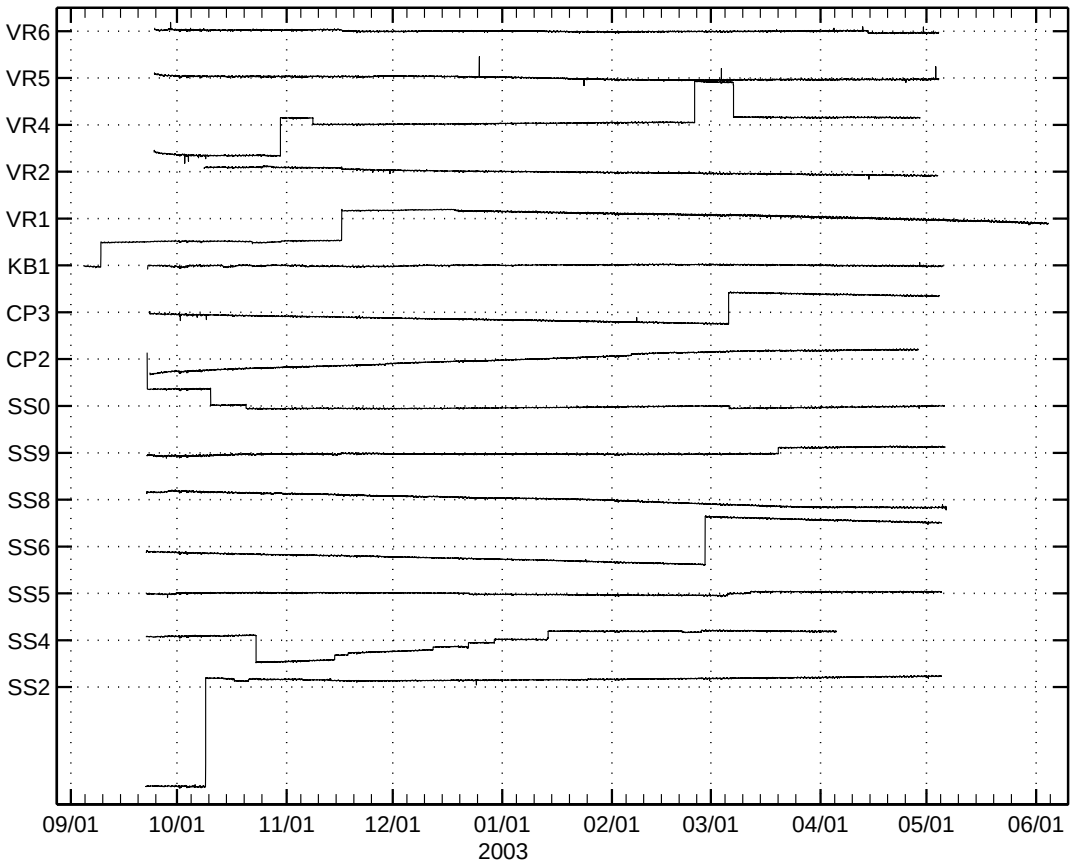

Fig. 10 — Vertical dotted lines indicate the beginnings of months (GMT). Horizontal dotted lines indicate means of the indicated ADCP heading records (solid lines); these means are offset from one another by 10°. SS10 is labeled as SS0 here and in the following figure for ease of display.

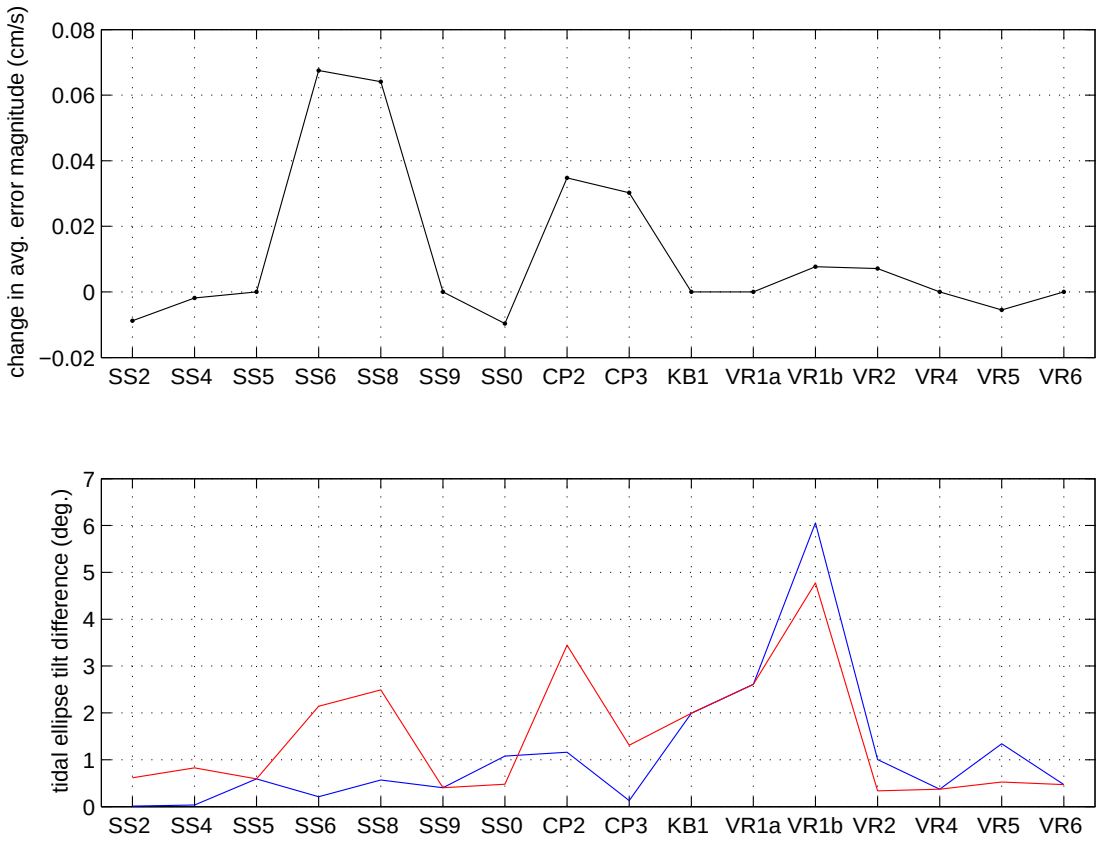

Fig. 11 — The top panel shows the average magnitude of the vector difference between tidal currents reconstructed using tidal coefficients from the first half analysis and the second half analysis for the case without compass drift corrections, minus the same quantity for the case with compass drift corrections. A positive value indicates that compass drift corrections decreased the differences in tidal currents. The bottom panel shows absolute differences in M_2 tidal current ellipse orientations from response analyses of the first and second halves of vertically-averaged current time series from JRP ADCPs. The red line is from analyses of time series without long-term compass drift corrections and the blue line is from analyses of time series with the correction.

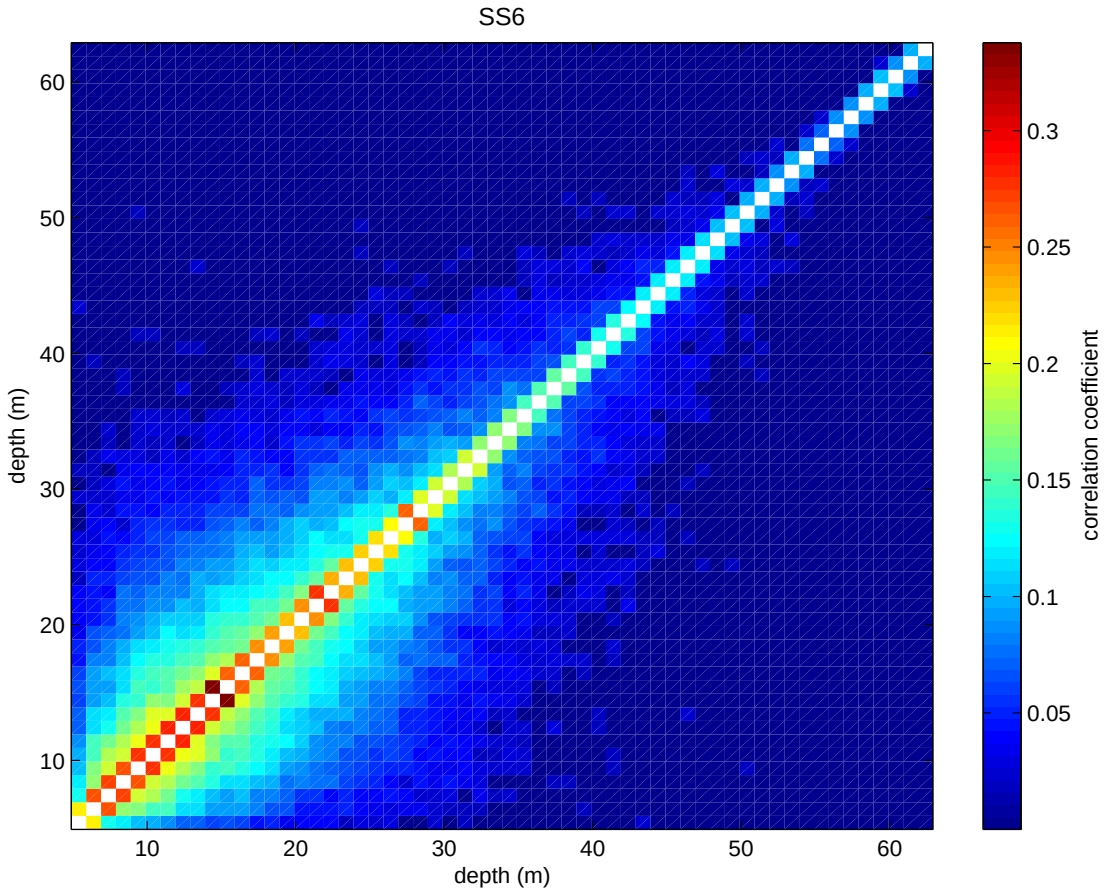

Fig. 12 — Calculated correlations at station SS6 between velocity error time series at different depth levels. The center diagonal is marked white since its position in the graph would indicate comparison of the same time series.